Rapid Prototyping J

A pilot study to assess an in-process inspection method for small diameter holes produced by Direct Metal Laser Sintering

Journal:	*Rapid Prototyping Journal*
Manuscript ID	RPJ-05-2019-0132.R2
Manuscript Type:	Original Article
Keywords:	Direct Metal Laser Sintering (DMLS) technology, small diameter holes, image processing software, quality control, empirical models

Postprint of: Deja, M. and Zielinski, D. (2019), "A pilot study to assess an in-process inspection method for small diameter holes produced by direct metal laser sintering", Rapid Prototyping Journal, Vol. 26 No. 2, pp. 418-436. DOI: 10.1108/RPJ-05-2019-0132

A pilot study to assess an in-process inspection method for small diameter holes produced by Direct Metal Laser Sintering

Purpose

The purpose of this research is to evaluate the geometric quality of small diameter holes in parts printed by DMLS technology. An in-process optical inspection method is proposed and assessed during a pilot study. The influence of the theoretical hole diameter assumed in a CAD system and the sample thickness (hole length) on the hole clearance was analysed.

Design/methodology/approach

The samples made of two different materials: EOS MaragingSteel MS1 and aluminium alloy EOS Aluminium consisted of straight through holes of different diameters and lengths. Dimensional and shape accuracy of the holes were determined with the use of the image processing software and the computer analysis of 2-D images. The definition of the equivalent hole diameter was proposed to calculate the hole clearance. Feret's diameters were determined for the evaluation of the shape accuracy.

Findings

The dependency between the equivalent hole diameter and the theoretical diameter was approximated by the linear function for a specific sample thickness. Additionally, a general empirical model for determining the hole clearance was developed, allowing for calculating the equivalent hole diameter as a function of a sample thickness and a theoretical hole diameter.

Practical implications

Developed functions can be used by designers for a proper assignment of a hole diameter to achieve the required patency. The relevant procedures and macros based on proposed empirical models can be embedded in CAD systems to support the designing process.

Originality/value

The analysis of the geometric quality of the holes in parts printed by DMLS was based on the computer analysis of 2-D images. The proposed method of assessing the shape accuracy of straight through holes is relatively cheap, is widely available and can be applied to the features of other shapes produced by 3D printing.

Keywords: Direct Metal Laser Sintering (DMLS) technology, small diameter holes, image processing software, quality control, empirical models

Paper type: Research paper

1. Introduction

Additive manufacturing methods, also commonly referred to as generative or incremental techniques, are currently one of the most dynamically developing methods of manufacturing and shaping products. Rapid Prototyping (RP) technology, as the name suggests, refers strictly to the production of prototypes and models of future products. Although the term is often used to describe incremental methods as a whole, it is now a somewhat outdated term. Dynamic development of incremental techniques related to, among others, the use of modern 3D printing systems (Zieliński, 2018-03), processing of modern materials, obtaining higher and higher dimensional and shape accuracy and later application of printed elements, requires the use of the term Rapid Manufacturing. This term indicates the possibility of making full-value elements or components with characteristics similar to those produced by conventional manufacturing techniques in a single or small series production (Gebhardt, 2013; Breuninger, 2012; Ahuja *et al.*, 2015). Currently used Rapid Prototyping/Rapid Manufacturing (RP/RM) technologies enable not only the production of prototypes and physical models of future products but are also used for short series production of technical spare parts or final components. Continuous development of RP/RM technologies allows for the realization of many promising applications in various fields. The number of innovative, optimally designed and manufactured elements is thus increasing the popularity and interest in 3D printing technology, both from the industrial sector and the customers themselves (Berman, 2012; Thompson *et al.*, 2016; Prakash *et al.*, 2018; Gebisa *et al.*, 2017). However, meeting high requirements of the modern market requires further development not only of the process itself and the types of processed materials, but also the design and building of entire production systems equipped with 3D printers (Eyers and Potter, 2017). The development of such an approach in the next few years may lead to the transformation of the incremental technology into a common production method. Apart from purely technical applications, incremental methods are also very often used in other areas, such as architecture, archaeology and even art. Currently, they are widely used in the medical industry, where they are used not only to produce three-dimensional structures and anatomical models, but also medical instruments (Hieu, 2005; Gu *et al.*, 2015; Popescu *et al.*, 2018). Additive manufacturing methods should be an integral part of the product development process (VDI 3405, 2014-12). The possibility

of making a prototype of a future product, already in the first phase of its development cycle, i.e. in the design phase, enables initial research to be performed for optimal design and to produce a high-value product. Such an approach not only allows for the shortening of development time and implementation of a new product on the market, but also minimizes the costs resulting from badly designed and manufactured elements.

A characteristic feature of 3D printing technology, which distinguishes it from traditional material removal methods, is the layered structure of the object created on the basis of its 3D model (ASTM, 2015). The geometry of the part designed in the CAD environment (usually in STL format) is transformed through specialized software into a series of machine commands, enabling printing of the previously modelled object. As a result of automatic overlapping of subsequent layers of material, a three-dimensional element is produced (Gibson *et al.*, 2014). It is also worth emphasizing that during the incremental process, apart from creating the geometry of the designed object, the mechanical properties of the part are constituted depending on the material type, the part orientation and working parameters of the 3D printing machine (Gebhardt, 2013; Thomas, 2009).

2. Characteristics of 3D printing powder technology

Currently used Rapid Prototyping/Rapid Manufacturing technologies are gaining more and more popularity due to their development and processing of modern materials. The development of particular 3D printing technologies and the improvements introduced to them allow for the making of increasingly durable and technologically advanced objects, which often have features similar to full-value products and final elements of industrial machines and equipment. The development of 3D printing systems also improves the obtained dimensional and shape accuracy, making it possible to print more precise and complex-shape objects, including miniature parts (Vaezi *et al.*, 2013).

3D printing technology can be classified into a number of methods, which are differentiated in part by the terms of constructing the physical model, type and form of the processed material, as well as the source of energy used in the incremental process (VDI 3405, 2014-12; Vayre *et al.*, 2012). Moreover, each of the incremental technologies make it possible to obtain, depending on the class of the applied 3D printing system and the type of a processed material, characteristic properties and the specific dimensional and shape accuracy of the printed objects. The most commonly used 3D printing methods are presented in Table 1, including considered in the paper DMLS technology, which can be implemented in many industrial

applications requiring precise printing of elements with complex-shape geometries and good mechanical properties.

Table 1. Most popular 3D printing technologies with the characteristics of the construction of the physical model and the source of energy generated for the incremental process.

Due to dynamic miniaturization, there is a strong demand for the construction of objects with complex microstructures, such as curved holes and canals of small dimensions. Currently used 3D printing technologies, including methods based on the photopolymerization process, such as stereolithography and DLP (Direct Light Processing) technology, allow for the building of miniature and precise objects with holes of small diameters (Bertsch *et al.*, 2000; Xu *et al.*, 2007; Davoudinejad *et al.*, 2018). Powder technologies of 3D printing, especially DMLS, also have great potential in the building of miniature elements.

DMLS technology belongs to the basic Powder Bed technology. Similar to other incremental technologies, its characteristics feature layered construction of the printed object, as a result of selective remelting of subsequent layers of powdered material. DMLS technology enables the building of objects of complex shapes, which are characterized by high and repeatable strength properties at the same time. A number of advantages and application possibilities increase the use of these types of elements in the industry. DMLS technology enables not only the building of prototypes and models of future objects. Currently, it is also successfully used in small series production of functional and final parts of machines and mechanical devices. The aerospace industry is one example of DMLS technology's tremendous potential. As the current research shows, this technology can be used to manufacture complex and responsible components of aircrafts (Zieliński, 2018-09). An unquestionable advantage of DMLS technology, used especially in the aerospace industry, is the ability to reduce the weight of manufactured components. For this reason, DMLS technology is widely used in topological optimization of aircraft parts (Zieliński, 2018-10). According to the current research, this approach allows for a significant reduction in the weight of manufactured components, which is associated with a smaller amount of material consumed during the production process and consequently leads to a reduction in the cost of their production. A wide spectrum of application capabilities of DMLS technology includes also building objects with complex-shape geometries, containing miniature elements in the form of small channels and holes. DMLS technology can be used to produce inserts for casting and injection moulds with so-called conformal cooling. Due to the complex systems of small cooling channels, the quality

of the manufactured part was improved and the duration of the injection cycle was shortened. DLMS technology was successfully used to produce drills with optimally designed internal cooling channels, without reducing the rigidity and strength of the drill (Tyczynski *et al.*, 2018). Other examples of RP/RM capabilities are the models of high-pressure blades of gas turbine stages and their particular components (Iftikhar *et al.*, 2013; Vaezi *et al.*, 2011; Sher, 2018; Gebisa and Lemu, 2018) made with the use of selected 3D printing technologies, including mainly the DMLS method. In addition to their complex geometry, such elements required the series of small diameter holes and channels supplying the coolant or generating longitudinal whirlpools – Figure 1 (Deja *et al.*, 2018; Zieliński, 2017; Flaszynski *et al.*, 2017).

Figure 1: Gas turbine blade: a) CAD model with 0.3 mm diameter holes, b) the working chamber of the 3D printer with a manufactured part (Zieliński, 2017)

The detection of holes with the use of a computer tomography and a digital radiography enabled the identification and measurement of the created features of the diameter greater than 0.3 mm. Micro-holes of the diameter 0.3 mm were not manufactured by DLMS and only their nucleuses were detected on the blade surface – Figure. 2.

Figure 2. Spots of forming the micro-holes of 0.3 mm diameter on blade surface: a) a nucleus of micro-hole, b) a tear-off on material surface (Deja *et al.*, 2018)

The nucleus of micro-hole and the defects of the material discontinuity, visible in the pictures from Figure 2, confirmed the problem of producing small holes and canals by RP/RM techniques.

Application of incremental technologies, including the above mentioned all powder methods, may eliminate many of the limitations of traditional manufacturing techniques e.g. producing inner features with complex shapes at any location in the part. For this reason, it is very important to determine the possibilities and limitations of DMLS technology in the production of components consisting of complex inner features especially with small dimensions.

Building complex geometries using 3D printing technology can cause many errors. The study of geometric accuracy, as one of the most important indicators of 3D printing product quality, has become the subject of many research works (He *et al.*, 2019; Huang *et al.*, 2015; Xu *et al.*, 2013; Huang *et al.*, 2014). Their source, regardless of the type of method, may be model or processing error. Many contemporary research works focus on the development of the quality

control methods for FDM technology, which is characterized by low and inconsistent geometric accuracy. For this reason a lot of different techniques not only for 3D printed parts, but also for 3D printing systems have been developed (Wu *et al.*, 2016; Yoon *et al.*, 2014; Wang *et al.*, 2017). In the paper (Tong *et al.*, 2008) authors focused on presenting the method of compensation of shape deviations by correcting slice files of the STL model. The methods of model error reduction by optimizing the STL model and adapting the layer thickness were discussed in (Pandey *et al.*, 2003; Zha and Anand, 2015). Another factor, which has a great influence on the quality of printed elements, is the optimization and proper selection of process parameters (Sood *et al.*, 2011; Mohamed *et al.*, 2016). In case of elements made of metal powders using RP/RM technologies the surface is characterized by high irregularities. Selection of an appropriate measurement method for this type of surface texture may therefore pose a challenge (Townsend *et al.*, 2016). In the case of holes with small diameters, additional difficulties are caused by numerous material defects in the form of discontinuities and cracks. For this reason, defect detection and quality control of metal powder processing is necessary. It is critical to develop an effective measurement method, which allows for obtaining reliable results and improving the production quality in the future, especially that designing even simple geometries like radii and holes for 3-D printing technologies becomes increasingly complex when compared to conventional processes, as shown by the example of Selective Laser Melting (SLM) technology in (Thomas, 2009).

The current measurement methods for features such as holes can use both contact and contactless measuring techniques. One of the most common methods for inspection of internal diameters is the use of GO and NOT GO fixed gages. During testing the GO gage slides into the hole, whilst the NOT GO gage must not go into the hole (Kalpakjian and Schmid, 2006). Although this type of measurement method is relatively cheap and easy to use, it does not provide precise information about the actual dimension of the inner feature.

Using a Coordinate Measuring Machine (CMM) with a touch probe is a more accurate method of measuring especially 3-dimensional geometries. The rough surfaces of printed test parts may cause the probe to touch at different heights of the peaks and also on the weld spatter (Thomas, 2009). Due to that, inaccurate and unrepeatable measurement results may occur influencing the limited applicability of touch probes as an in-process inspection method especially for small features.

The measurements of produced inner features can be realised with the use of other advanced measuring techniques such as the computer tomography or the digital radiography (Deja *et al.*, 2018) which are quite expensive and not always available in the production space

equipped with 3-D printers. Notwithstanding, the computer tomography or the digital radiography can be the only method for measuring and inspecting complex features or long small holes inside a workpiece.

Optical inspections with the use of microscopes or visual cameras have the capability to show the surface characteristics as well as to measure very fine details, shapes, and dimensions on small workpieces. The formation of elevated regions in the part were examined in (Kleszczynski et al., 2012; Zur Jacobsmühlen et al., 2013) with the use of visual cameras. Image processing algorithms were implemented by Aminzadeh and Kurfess in (Aminzadeh and Kurfess, 2015) to automatically detect, from high-resolution camera images, the geometric errors and inspect the dimensional accuracy of the part. Capturing in-situ images from every layer of the laser powder-bed fusion process allowed for developing an online monitoring system for quality of fusion and defect formation in every layer of the manufactured part (Aminzadeh and Kurfess 2019). The developed statistical Bayesian classifier was able to detect, within each layer, regions and portions of the layer that had low quality of fusion with high chances of defect formation.

The authors of the article attempted to develop a reliable, relatively simple and cheap method of assessing the quality of small diameter holes made by the DMLS technology. The required cross sectional area was assumed as the main acceptance criteria for cooling channels. The dimensions of the holes in test parts examined by Thomas in (Thomas, 2009) were also set according to cross sectional areas assuming that the holes used as cooling channels would have to manage calculated and required amounts of fluid flow. Furthermore, the surface roughness is another important criteria influencing the resistance of the fluid flow. As validated in (Thomas, 2009; Dzionk, 2010) the vertically oriented surface has the lowest roughness, so the hole axis orientation at 90°, perpendicular to the substrate plate, was chosen to make all holes. The layers of a part were built up one on top of another in the z-axis to achieve the lowest and, theoretically, equal surface roughness for all holes.

The current measurement methods used in RP technologies focus on the examination of the whole layer and elevated regions as well as surface characteristics by means of the processing high-resolution camera images. A large range of data that can be obtained from microscope or visual camera images allows for providing reliable information about defects of parts or process errors of 3-D printing systems that can lead to part defects. Considering the above and the possible applicability of presented and discussed other measuring methods, the optical inspection was chosen as the most suitable method for examining the cross sectional areas of

printed holes. The limitations associated with making small features were determined by the authors with the use of the computer analysis of 2-D images taken by a stereoscopic microscope and analysed by an image processing software. Shadowgraph images analysed in (Thomas, 2009) also provided good visual evidence of the deformation that occurs in holes and created an accurate two-dimensional representation of the hole cross sections. Nevertheless, a method presented in the article is faster and more accurate than the inspection with the shadowgraph's optical measurement system and CAD software, when all parts were measured at 10 times magnification. The authors' method allows for inspecting the hole sectional area (the clearance area) at up to 80 times magnification which is a reliable value for dimensions of cooling channels with a typical tolerance grade higher than H10 as they are not to be mated with another part.

During the inspection, the Feret's diameters were determined for the evaluation of the shape accuracy. The measured cross sectional areas allowed for calculating an equivalent diameter of holes which could be used as circular or non-circular cooling channels of the specified clearance. The dependencies between the measured diameters and the theoretical diameters were approximated by the linear function. Additionally, a general model was developed, allowing for the calculation of the hole clearance as a function of a sample thickness and a theoretical hole diameter. Detailed information on the proposed method together with the analysis of obtained results are presented in the further part of the article. The developed method was used for the assessment of straight through holes but after implementing appropriate image processing algorithms it could be applied to the features of other shapes produced by 3D printing. The results of the proposed inspection method can help with making decisions regarding the acceptance of the built geometries and taking corrective actions in a CAD system to achieve required cross sectional areas.

3. Research methodology

Subsequent stages of the proposed procedure for the quality evaluation of the straight through holes are presented in Figure 3. The microscopic observations with the use of a stereoscopic microscope were carried out after manufacturing test samples on a 3D printer. The image processing software was used in order to improve the sharpness of taken images and to conduct the measurements. The final stage of the procedure was the formulation of equations describing the expected diameter of a hole manufactured on a 3D printer. This diameter was expressed as a linear function of a diameter specified in a CAD model. The defined function

can be used to determine the appropriate dimension values in order to obtain the features of the required shape and size.

Figure 3. Scheme of the adopted research methodology

3.1. Test samples

Test samples manufactured by DMLS technology consisted of vertically made straight through holes of varying diameters and lengths. In the first set of samples straight through holes of diameters ranging from 1 mm to 5 mm were designed in a cubic sample of a height of 10 mm – Figure 4.

Figure 4. Drawing of a test sample with holes of diameters ranging from 1 mm to 5 mm

Test samples presented in Figure 5 were produced using the EOSINT M280 machine along with the process parameters presented in Table 2 and applied to make all samples. Two different powder materials were selected to make the parts: EOS MaragingSteel MS1 (EOS GmbH - Electro Optical Systems, 2011) and aluminium alloy EOS Aluminium AlSi10Mg (EOS GmbH - Electro Optical Systems, 2014). Smaller holes with diameters ranging from 0.3 mm to 1.5 mm were designed in the next set of samples with variable thickness: G = 1 mm; 2 mm; 4 mm; and 5 mm – Figure 6.

Figure 5. Samples made of EOS MaragingSteel MS1 (a) and aluminium alloy EOS Aluminium (b) with relevant digital models obtained by a computer tomography

Table 2. Additive process parameters used for printing the test samples.

Figure 6. Straight through holes designed in a sample of a variable thickness: G = 1 mm, 2 mm, 4 mm and 5 mm

The samples presented in Figure 6. were made only of aluminium alloy EOS Aluminium AlSi10Mg. When the building process was completed, the samples were mechanically separated from the working platform. Finally, the unmelted powder was cleaned off the samples and the outer sharp edges were chamfered.

4. Qualitative research

The qualitative evaluation allowed for the identification of the shape and material defects in printed holes. A stereoscopic microscope Stemi 2000-C from Zeiss with dedicated AxioVision SE64 software was used for the microscopic observations of test samples and for taking several images after focusing on a different part of the hole. Focus stacking software Helicon Focus 6.8.0 was used for a post-processing technique to extend the depth of field in the images after blending all the sharp areas together. That processing allowed for producing a completely sharp image, as it is seen in Figure 7 presenting the exemplary hole made of EOS Aluminium AlSi10Mg material.

Figure 7. Images of the hole before (a) and after (b) a focus stacking

Combining images with different degrees of focus allowed for obtaining high quality images with detailed views of material defects. The sharp images were obtained after a focus stacking was used to determine the dimensional and shape accuracy. All images presented in the further part of the article were post processed by Helicon Focus 6.8.0 software. Figure 8 and Figure 9 show post processed images of holes in 10 mm thick test samples made of EOS MaragingSteel MS1 and EOS Aluminium AlSi10Mg respectively.

Figure 8. Test sample made of EOS MaragingSteel MS1 with holes of assumed diameters of: a) 5 mm, b) 4 mm, c) 3 mm, d) 2 mm and e) 1 mm

Figure 9. Test sample made of EOS Aluminium AlSi10Mg with holes of assumed diameters of: a) 5 mm, b) 4 mm, c) 3 mm, d) 2 mm and e) 1 mm

As it can be seen in Figure 8 and Figure 9, the use of DMLS technology allowed for building all the designed inner features, although the contours of the holes strongly depended on the material type. Samples made of MS1 material are characterised by better shape accuracy in comparison to samples made of EOS Aluminium material with larger contour irregularities. Besides, the observations of the obtained images indicated the defects in the form of changes in the material structure along the holes' edges. Quantitative measurements presented in the next chapter confirmed the initial conclusions from the microscopic observations that the

diameters of the printed holes were smaller than the designed diameters, mainly due to the identified defects.

An analogous study with an image processing was carried out for the second set of thinner samples with the holes of smaller diameters – Figure 6. Figure 10 shows the contours of the smallest hole (0.3 mm) made in samples of a different thickness.

Figure 10. Test samples made of EOS Aluminium AlSi10Mg material with holes of an assumed 0.3 mm diameter and a variable thickness: a) 1 mm, b) 2 mm, c) 4 mm and d) 5 mm

The analysis of the images indicated the differences between the obtained and assumed shapes and diameters. The material defects in the form of tears and burrs were identified especially in a 1 mm thick test sample – Figure 11. Additionally, more material structure defects were identified, in comparison with a constant thickness sample made of the same material. The observations of microscope images have indicated that reducing the diameter and length of holes affected an increased number of material defects.

Figure 11. The 1 mm thick test sample manufactured from EOS Aluminium AlSi10Mg material with holes of assumed diameters: a) 1 mm, b) 0.9 mm, c) 0.8 mm and d) 0.7 mm

The structural changes and material defects caused the differences between the theoretical (assumed) and measured diameters. In addition, the material discontinuities inside the holes confirmed the lack of a full material melting.

The series of images processed by Helicon Focus 6.8.0 software allowed for conducting a preliminary quality assessment of manufactured holes and the identification of the material defects by the means of inspection. The proposition of the quantitative analysis of the dimensional and shape accuracy of printed holes is presented in the next chapter.

5. Quantitative research

5.1. Holes in samples of constant thickness

The quantitative analysis of the dimensional and shape accuracy of printed holes was carried out with the use of the software for image processing and measuring the graphical objects [Matlab, 2018]. The determination of the hole clearance was the first step of the analysis – Figure 12. The clearance influences the patency of the hole and the flow rate of a various

media e.g. the coolant flow in the internal channels of the cutters or turbine blades [Tyczynski *et al*., 2018, Deja *et al*., 2018]. The surface area of the hole clearance was calculated on the basis of the number of corresponding pixels from the yellow region - Figure 12 b. The size and shape of this area depend on the material defects which may significantly reduce the hole clearance.

Figure 12. The sample made of MS1 material with the hole of an assumed diameter d_t = 3 mm: a) top view of the hole before the measurements, b) top view of the hole after the determination of its clearance area and Feret's diameters: horizontal d_h and vertical d_v; d_e – equivalent hole diameter

A formula derived from a circle surface area was used to calculate the diameter d_e of an ideal circular hole whose area A_e is equal to the clearance area A_c:

$$A_e = A_c = \frac{\pi {d_e}^2}{4}, \tag{1}$$

$$d_e = 2\sqrt{\frac{A_c}{\pi}}, \tag{2}$$

where:

A_c – hole clearance area determined by an image processing software,

A_e – circular hole area equal to the hole clearance A_c,

d_e – equivalent hole diameter.

Additionally, the vertical d_v and horizontal d_h Feret's diameters were determined by an image processing software - Figure 11 b. For the size and shape evaluation, calculated diameters d_e, d_v and d_h were compared to a theoretical diameter d_t, assigned in a CAD model. Depending on the values of diameters, different cases can be identified according to the following conditions:

I. $d_e = d_h = d_v = d_t$: full theoretical clearance, no shape error, (3)

II. $d_e = d_t \wedge (d_e \neq d_v \vee d_e \neq d_h)$: full theoretical clearance, shape error, (4)

III. $d_e \neq d_t \wedge (d_e \neq d_v \vee d_e \neq d_h)$: clearance difference, shape error, (5)

where:

d_t – theoretical diameter assigned in a CAD model,

d_v – vertical Feret's diameter,

d_h – horizontal Feret's diameter.

The absolute Δd and relative δ_d diameter errors were calculated using the following formulas:

$$\Delta d = d_t - d_e \,, \tag{6}$$

$$\delta_d = (\Delta d / d_t) \cdot 100\%. \tag{7}$$

Table 3 presents the calculated diameters and errors for a 10 mm thick test sample made of MS1 material. The results indicate big differences between the theoretical and calculated diameters. The condition no. III of the clearance difference and shape error was met for each hole – Equation 5. The smallest absolute error was achieved for a hole of $d_t = 1$ mm, and the largest one for a hole of $d_t = 4$ mm. The absolute errors are at a similar level therefore the relative error decreases with the increase in a diameter d_t.

Table 3. Analysed diameters and errors for a 10 mm thick test sample made of MS1 material.

For the shape evaluation, the horizontal and vertical Feret's diameters were compared to the diameters d_e of the equivalent holes – Figure 13.

Figure 13. Hole diameters d_e, d_v, d_h determined for a 10 mm thick test sample made of MS1 material

It can be seen in Figure 13 that there are differences between the Feret's diameters and the calculated diameter d_e. Even small deviations between these dimensions indicate the shape errors especially the roundness error of the feature being produced. For an ideal round contour, all three diameters should be the same. The calculated differences, as well as the visual assessment of the images of individual holes, indicated that the round shape had not been fully obtained for any of the holes. As it was expected, all diameters d_e, d_v and d_h were smaller than the theoretical diameter d_t assigned in a CAD model and d_e was smaller than d_v and d_h.

An analogous procedure and calculations were carried out for the assessment of the dimensional and shape accuracy of holes produced in an aluminium alloy sample - Figure 14. As for the sample made of MS1, the condition no. III (differences in the diameters) has been met, indicating the holes inaccuracy – Table 4. The smallest absolute Δd error was achieved for a hole of $d_t = 1$ mm, and the largest one for a hole of $d_t = 5$ mm. Contrary to the sample made of MS1 material, the relative errors δ_d are at a similar level due to the increase in the absolute error Δd with the increase in a theoretical diameter d_t – Figure 15.

Figure 14. The sample made of aluminium alloy with the hole of an assumed diameter $d_t = 2$ mm: a) top view of the hole before the measurements, b) top view of the hole after the determination of its clearance and Feret's diameters: horizontal d_h and vertical d_v

Table 4. Analysed diameters and errors for a 10 mm thick test sample made of EOS Aluminium AlSi10Mg material.

Figure 15. Relative errors of the hole diameter for a 10 mm thick test sample

In the comparison to the samples made of MS1 material, the EOS Aluminium AlSi10Mg material allowed for obtaining a higher dimensional accuracy for the diameters ranging from $d_t = 1$ mm to $d_t = 4$ mm.

The differences between the diameters d_e, d_v and d_h (Figure 16) indicate that the resulting internal profiles do not have a fully circular shape, similarly to the samples made of MS1 material (Figure 13).

Figure 16. Hole diameters d_e, d_v, d_h determined for a 10 mm thick test sample made of EOS Aluminium AlSi10Mg material

5.2. Small-diameter holes in samples of different thickness

The developed measurement procedure was applied for determining the dimensional and shape accuracy of the small-diameter holes in the samples whose thickness $G = 1$ mm; 2 mm; 4 mm; and 5 mm (Figure 6), made of EOS Aluminium AlSi10Mg material. Calculated with the Equation 6, the absolute diameter errors for the diameter d_t ranging from 0.3 mm to 1.5 mm, are presented in Figure 17.

Figure 17. Absolute errors of the hole diameter for a test sample made of EOS Aluminium AlSi10Mg material for the thickness G of: a) 1 mm, b) 2 mm, c) 4 mm, and d) 5 mm

The graphs in Figure 17 show an upward trends of the absolute error that increases when the theoretical diameter increases. However, there are clear deviations from the trend line, especially for a 1 mm thick sample, characterised by a very low value of the coefficient of determination R^2, as the material defects significantly reduced the clearance of small holes.

Relative errors of the theoretical diameters d_t ranging from 0.3 mm to 1.5 mm were calculated using the formula 7 and are presented in Figure 18. The holes in the thinnest sample are characterised by the biggest errors while for other samples the errors are below 25%. This confirmed the difficulty in the manufacturing of thin parts, which is associated with a greater risk of numerous defects, affecting the dimensional and shape accuracy.

Figure 18. Relative errors of the theoretical hole diameter d_t for a test sample of a different thickness, made of EOS Aluminium AlSi10Mg material

5.2.1. Regression equations for determining a hole diameter

The prediction of a hole clearance is a crucial task for designing the internal features in mechanical components, especially with a limited or even no access to the feature during post-processing for improving its shape and size. Fitting mathematical equations to experimental data can help in a better assignment of a theoretical diameter d_t in CAD models used for producing a feature with the required clearance in real parts. According to the tendencies in obtained results presented in Figure 16, the dependencies between the calculated diameters d_e, d_v, d_h and the theoretical diameter d_t, were approximated by the linear function:

$$\hat{y} = a \cdot d_t, \tag{8}$$

where:

$\hat{y}$ – the expected value of a diameter d_e, d_v, or d_h,

a – the directional coefficient of the regression function.

The fitting of the empirical data to the proposed function was estimated on the basis of the coefficient of determination R^2:

$$R^2 = \frac{\sum_{i=1}^{n} (\hat{y}_i - \bar{y})^2}{\sum_{i=1}^{n} (y_i - \bar{y})^2}, \tag{9}$$

where:

y_i - the value of a diameter d_e, d_v, or d_h for the hole no i,

$\bar{y}$ - arithmetic mean of diameters,

n - the number of holes.

The maximum absolute error Δy_{max}, the maximum relative error δ_{max} and the root mean squared error RMSE were calculated using the appropriate formulas:

$$\Delta y_{max} = max|y_i - \hat{y}_i|, \tag{10}$$

$$\delta_{\max} = \max\left(\frac{|y_i - \hat{y}_i|}{y_i}\right)100\%, \tag{11}$$

$$RMSE = \sqrt{\frac{1}{n}\sum_{i=1}^{n}(\hat{y}_i - y_i)^2}\ . \tag{12}$$

The proposed function for calculating a diameter d_e enabled good fitting of experimental data especially when the holes were made in samples of a thickness $G \geq 2$ mm. As it is seen in Figure 19 and Table 5, when the sample thickness increased, a coefficient of determination R^2 also increased and the maximum relative error $\delta_{\max}$ decreased. As a result of material defects in holes of smaller diameters, the linear functions determined for the thinnest sample were characterized by the worst fitting with the biggest $\delta_{\max}$ and RMSE errors of a diameter d_e (Table 5) and Feret's diameters (Table 6).

Figure19. Linear fitting of analysed hole diameters for samples made of EOS Aluminium AlSi10Mg material for a thickness G of: a) 1 mm, b) 2 mm, c) 4 mm, and d) 5 mm

Table 5. Parameters of a function for determining equivalent hole diameter $d_e = a \cdot d_t$, $d_t \in$ [0.3, 1.5]

Table 6. Parameters of a function for determining Feret's diameters $d_h = a \cdot d_t$ and $d_v = a \cdot d_t$, $d_t \in$ [0.3, 1.5]

5.2.2. A general model for determining a hole clearance

As it can be seen in Table 5, the value of a directional coefficient a of a function for determining an equivalent hole diameter d_e increased with the increase in a sample thickness G. The relationship between the directional coefficient a and the sample thickness G was approximated by the power function:

$$\hat{a} = b \cdot G^c, \tag{13}$$

where:

$\hat{a}$ – the expected directional coefficient of the linear regression function,

G – thickness of the sample,

b, c – coefficients of a power function.

The assumed approximation function for the analysed range of a theoretical diameter $d_t \in [0.3, 1.5]$, with estimated values of b and c is given as:

$$\hat{a} = 0.78 \cdot G^{0.07}, \text{ for } G \in [1, 5]. \quad (14)$$

The Equation 14 is characterized by a good curve fitting with a coefficient of determination R^2 close to 1 – Figure 20.

Figure 20. The relationship between a sample thickness (hole length) G and the directional coefficient of a linear function for calculating the equivalent hole diameter d_e; —— the coefficient $\hat{a}$ for the intervals of G and d_t used for modelling, $G \in [1, 5]$, $d_t \in [0.3, 1.5]$; ····· the coefficient $\hat{a}$ for the extended interval of G and d_t

5.2.3. Experimental validation of proposed models

For the experimental validation of the proposed model, a 3 mm thick sample made of EOS Aluminium AlSi10Mg material was produced with thirteen holes whose diameter d_t = 0.3 ÷ 1.5 mm. An expected directional coefficient $\hat{a} = 0.843$ was calculated with Equation 14 for $G = 3$ mm – Figure 20, Table 7. The predicted equivalent hole diameter $\hat{d}_{e1}$ was calculated using the following formulae, based on Equation 8 and Equation 14:

$$\hat{d}_{e1} = \hat{a} \cdot d_t, \quad (15)$$

$$\hat{d}_{e1} = 0.78 \cdot G^{0.07} \cdot d_t, \quad \text{for } G \in [1, 5],\ d_t \in [0.3, 1.5], \quad (16)$$

$$\hat{d}_{e1} = 0.843 \cdot d_t, \quad \text{for } G = 3,\ d_t \in [0.3, 1.5]. \quad (17)$$

The values of an equivalent hole diameter d_e were obtained according to the procedure presented in Chapter 5.1, after the microscopic measurements of the produced holes with the use of an image processing software - Figure 21. The maximum absolute error Δy_{max}, the maximum relative error δ_{max} and the root mean squared error RMSE for obtained d_e and expected $\hat{d}_{e1}$ were calculated (Table 7, for G = 3 mm and $\hat{a} = 0.843$) using the appropriate Equations 10, 11, 12.

Furthermore, the obtained values of d_e for $G = 3$ mm (Figure 20) were fitted to a single straight line for which the directional coefficient $a = 0.871$ was estimated - Figure 20, Table 7. The expected diameter $\hat{d}_{e2}$ for a coefficient $a = 0.871$ was calculated with the formulae based on Equation 8:

$$\hat{d}_{e2} = a \cdot d_t, \quad (18)$$

$$\hat{d}_{e2} = 0.871 \cdot d_t, \quad \text{for } G = 3,\ d_t \in [0.3, 1.5]. \tag{19}$$

The relevant errors Δy_{max}, δ_{max} and RMSE for obtained d_e and expected $\hat{d}_{e2}$ were also calculated (Table 7, for G = 3 mm and $a = 0.871$) using the appropriate Equations 10, 11, 12. Relatively small errors achieved for both coefficients a and $\hat{a}$ indicate that the Equation 16, assumed as an approximation function for the analysed range of a theoretical diameter $d_t \in [0.3, 1.5]$ and for the sample thickness $G \in [1, 5]$, can be a good tool for predicting the equivalent hole diameter d_e, effecting the hole clearance.

Table 7. Parameters of the linear function for calculating the equivalent hole diameter d_e for a 3 mm thick sample ($d_t = 0.3 \div 1.5$ mm) and 10 mm thick samples ($d_t = 1 \div 5$).

Additionally, the usefulness of the Equation 16 was verified for the values of variables which were out of the assumed ranges. Extended intervals of $G \in [1, 10]$ and $d_t \in [0.3, 5]$ corresponded to the dimensions of the examined test sample of the thickness $G = 10$ mm. The full range of analysed variables is presented in Figure 22, including the data for the samples made of two different materials: MS1 - data from Table 3 and AlSi10Mg - data from Table 4. The errors Δy_{max}, δ_{max} and RMSE of a diameter d_e that occurred for both coefficients a and $\hat{a}$ (Table 7) and data presented in Figure 20 and Figure 22 confirmed that Equation 16 enabled a good prediction of a diameter d_e, even for extended intervals of variables d_t and G. The biggest errors occurred for MS1 material, different than the one used for the model evaluation and validation. Similarly as for the thickness of $G = 3$ mm, errors were smaller for the coefficient a which was estimated for a diameter d_e fitted to a single straight line assumed as an approximation function of a specified variables d_t and G.

Figure 21. Obtained and predicted equivalent hole diameter d_e for a sample thickness $G \in [1, 5]$ and a theoretical hole diameter $d_t \in [0.3, 1.5]$

Figure 22. Obtained and predicted equivalent hole diameter d_e for the extended intervals of a sample thickness $G \in [1, 10]$ and a theoretical hole diameter $d_t \in [0.3, 5]$

Conclusions

The prediction of a hole clearance is a crucial task for designing the internal geometries in mechanical components, especially with limited or even no access to a feature during post-processing for improving its shape and size. The proposed in-process inspection method for the evaluation of the dimensional and shape accuracy of straight through holes was applied to AlSi10Mg and MS1 test samples manufactured by DMLS technology under the given process parameters. The hole clearance, influencing the feature patency, was determined by the software for an image processing. On the basis of the clearance area, the equivalent hole diameter d_e was calculated. Additionally, the vertical d_v and horizontal d_h Feret's diameters were determined. For the size and shape evaluation, calculated diameters d_e, d_v and d_h were compared to a theoretical diameter d_t, assigned in a CAD model used for producing a feature with the required clearance in real parts. Main conclusions from the performed research could be drawn as follows:

- The developed measuring method allowed for the optical inspection of a hole sectional area. All determined diameters d_e, d_v and d_h were smaller than the theoretical diameter d_t assigned in a CAD model due to the fact that a required cross sectional area and the round shape were not obtained for any of the holes.
- The difficulties in making small-diameter holes in AlSi10Mg thin plates were confirmed by the descriptive analysis carried out with the use of mathematical equations. According to the tendencies in obtained results, the dependencies between the diameters d_e, d_v, d_h and the theoretical diameter d_t, were approximated by a linear function for a definite sample thickness G (hole length) selected from the range $G \in [1, 5]$ and for an interval of a theoretical diameter $d_t \in [0.3, 1.5]$. When the sample thickness increased, the coefficient of determination R^2 also increased and the maximum relative error δ_{max} decreased. A linear function determined for the thinnest sample ($G = 1$ mm) was characterized by the worst data fitting with the biggest δ_{max} and RMSE errors.
- A general model for determining the hole clearance was also developed, allowing for the calculation of an equivalent hole diameter d_e as a function of the sample thickness $G \in [1, 5]$ and the theoretical hole diameter $d_t \in [0.3, 1.5]$. Additionally, for approximate calculations a developed model was applied to MS1 material and to the extended intervals of variables $G \in [1, 10]$ and $d_t \in [0.3, 5]$. Notwithstanding the above, estimated diameters were characterised by relatively small errors.

- The qualitative evaluation indicated that reducing the hole diameter and length increased a number of material defects which along with structural changes affected the differences between the theoretical (assumed) and determined diameters. The material discontinuities inside the holes, characterised by the lack of the full material melting, confirmed the difficulties in making small-diameter holes especially in thin plates.

Obtained results and accurate curve fitting enable utilisation of the proposed inspection method and models in further scientific research and in industrial practice. A large range of data that can be obtained from microscope images allows for providing reliable information about certain characteristics or features, such as dimensions, surface finish, and defects. The main areas for the potential use of a developed method, arising from the possibility of obtaining reliable data from the optical inspection with the use of a stereoscopic microscope, are as follows:

- The proposed in-process optical inspection method can help with making decisions regarding the acceptance of the built geometries and taking corrective actions in a CAD system to meet the design specification. Developed mathematical functions can be used by designers for a better assignment of diameters to achieve the required patency of holes which used as cooling channels have to manage calculated and required amounts of fluid flow. The relevant procedures and macros embedded in a CAD software will support the hole designing process for 3-D printing technologies.
- The inspection of qualitative characteristics, such as defects in printed parts, generally requires a larger sample size than for variables-type data. After implementing appropriate image processing algorithms, the developed measuring method can be feasible and economical even for 100 percent automated inspection of all printed parts, especially that the surface quality even for the same or a similar printed geometry can vary significantly. The increased sample size will allow for the statistical analysis of the data to be performed at the level of individual geometries for a wider spectrum of printed parts. The developed method can also be used in other rapid manufacturing systems and for non-metallic materials.
- The identified relationships can be applicable to a broader range of geometries, such as radii or round shapes, printed at the same orientation. They can also be used as

guidelines for making pilot holes when a high accuracy or secondary processing such as tapping a thread or reaming are required.

- Further research will focus on the examination of the wider spectrum of materials and the optimisation of process parameters to build a universal model, also for printing angulated holes. This will require a detailed investigation of how the printing parameters influence the surface finish which affects the resistance of the flow in cooling channels. The influence of the angle of the hole axis on the final diameters will be checked using the measurements based on a computer tomography and on the modified methodology presented in the paper.

Acknowledgments

The authors of the article would like to thank Dr. Piotr Pawłowski from the Department of Intelligent Technologies, the Institute of Fundamental Technological Research, Polish Academy of Sciences, for preparing the test samples. Special thanks to Dr. Tomasz Seramak from the Department of Materials Engineering and Bonding, Faculty of Mechanical Engineering, Gdansk University of Technology, for providing digital models of the test samples obtained by a computer tomography. Computations carried out with the use of software and computers from Academic Computer Centre in Gdansk - TASK (http://www.task.gda.pl).

References

1. Ahuja, B., Karg, M., Schmidt, M. (2015), "Additive manufacturing in production: challenges and opportunities", *In Laser 3D Manufacturing II. International Society for Optics and Photonics,* Vol. 9353, p. 935304.

2. Aminzadeh, M. and Kurfess, T. (2015), "Layerwise automated visual inspection in laser powder-bed additive manufacturing", In *ASME 2015 international manufacturing science and engineering conference* (pp. V002T04A011-V002T04A011). American Society of Mechanical Engineers.

3. Aminzadeh, M., Kurfess, T. R. (2019), "Online quality inspection using Bayesian classification in powder-bed additive manufacturing from high-resolution visual camera images". *Journal of Intelligent Manufacturing*, Vol. 30, Issue 6, pp 2505–2523.

4. ASTM (2015), ASTM52900-15, "Standard Terminology for Additive Manufacturing—General Principles—Terminology", *ASTM International, West Conshohocken, PA*.

5. Berman, B. (2012), "3-D printing: The new industrial revolution", *Business horizons*, Vol. 55 No. 2, pp. 155-162.

6. Bertsch, A., Bernhard, P., Vogt, C., Renaud, P. (2000), "Rapid prototyping of small size objects". *Rapid Prototyping Journal*, Vol. 6 No. 4, pp. 259-266.

7. Breuninger, J., Becker, R., Wolf, A., Rommel, S., Verl, A. (2012), *Generative Fertigung mit Kunststoffen: Konzeption und Konstruktion für Selektives Lasersintern*. Springer-Verlag, Berlin Heidelberg.

8. Davoudinejad, A., Péreza, L. D., Quagliotti, D., Pedersen, D. B., Garcíaa, J. A. A., Yagüe-Fabra, J. A., Tosello, G. (2018), "Geometric and Fature Size Design Effect on Vat Photopolymerization Micro Additively Manufactured Surface Features", *In Special Interest Group Meeting: Additive Manufacturing: Advancing Precision in Additive Manufacturing. The European Society for Precision Engineering and Nanotechnology.*

9. Deja, M., Dobrzyński, M., Flaszyński, P., Haras, J., Zieliński, D. (2018), "Application of rapid prototyping technology in the manufacturing of turbine blade with small diameter holes", *Polish Maritime Research*, Vol. 25 No. S1, pp. 119-123.

10. Dzionk, S. (2010). Surface Roughness Model for Components Created by Stereolithography Method. In *Solid State Phenomena*, Vol. 165, pp. 268-273. Trans Tech Publications.

11. EOS GmbH - Electro Optical Systems (2011), "EOS MaragingSteel MS1", available at: https://drukarki3d.pl/wp-content/uploads/2015/09/karta-materia%C5%82owa-EOS-MaragingSteel-MS1-ENG.pdf (accessed 12 November 2018).

12. EOS GmbH - Electro Optical Systems (2014), "EOS Aluminium AlSi10Mg", available at: https://drukarki3d.pl/wp-content/uploads/2015/09/karta-materia%C5%82owa-EOS-Aluminium-AlSi10Mg-ENG.pdf (accessed 12 November 2018).

13. Eyers, D. R., Potter, A. T. (2017), "Industrial Additive Manufacturing: A manufacturing systems perspective", *Computers in Industry*, Vol. 92-93, pp. 208-218.

14. Flaszynski, P., Doerffer, P., Piotrowicz, M. (2017), "Effect of Jet Vortex Generators on Shock Wave Induced Separation on Gas Turbine Profile", *Proceedings of the 13th International Symposium on Experimental Computational Aerothermodynamics of Internal Flows, 7-11 May 2017, Okinawa, Japan.*

15. Gebhardt, A. (2013), *Additive Manufacturing und 3D Drucken für Prototyping-Tooling-Produktion*, Carl Hanser Verlag, München.

16. Gebisa, A. W., Lemu, H. G. (2017), "Design for manufacturing to design for Additive Manufacturing: Analysis of implications for design optimality and product sustainability", *Procedia Manufacturing*, Vol. 13, pp. 724-731.

17. Gebisa, A. W., Lemu, H. G. (2018). "Additive Manufacturing for the Manufacture of Gas Turbine Engine Components: Literature Review and Future Perspectives", In *ASME Turbo Expo 2018: Turbomachinery Technical Conference and Exposition* (pp. V006T24A021-V006T24A021). *American Society of Mechanical Engineers.*

18. Gibson, I., Rosen, D. W., Stucker, B. (2014), *Additive manufacturing technologies*, Springer, New York, NY.

19. Gu, Q., Hao, J., Lu, Y., Wang, L., Wallace, G. G., Zhou, Q. (2015), "Three-dimensional bio-printing", *Science China Life Sciences*, Vol. 58 No. 5, pp. 411-419.

20. He, K., Zhang, Q., Hong, Y. (2019), "Profile monitoring based quality control method for fused deposition modeling process", *Journal of Intelligent Manufacturing*, Vol. 30 No. 2, pp. 947-958.

21. Hieu, L. C., Zlatov, N., Vander Sloten, J., Bohez, E., Khanh, L., Binh, P. H., Toshev, Y. (2005), "Medical rapid prototyping applications and methods", *Assembly Automation*, Vol. 25 No. 4, pp. 284-292.

22. Huang, Q., Nouri, H., Xu, K., Chen, Y., Sosina, S., Dasgupta, T. (2014), "Predictive modeling of geometric deviations of 3d printed products-a unified modeling approach for cylindrical and polygon shapes", In *2014 IEEE International Conference on Automation Science and Engineering (CASE)* (pp. 25-30). IEEE.

23. Huang, Q., Zhang, J., Sabbaghi, A., Dasgupta, T. (2015), "Optimal offline compensation of shape shrinkage for three-dimensional printing processes", *Iie transactions*, Vol. 47 No. 5, pp. 431-441.

24. Iftikhar, A., Khan, M., Alam, K., Imran Jaffery, S. H., Ali, L., Ayaz, Y., Khan, A. (2013), "Turbine blade manufacturing through rapid tooling (RT) process and its quality inspection", *Materials and Manufacturing Processes*, Vol. 28 No. 5, pp. 534-538.

25. Kalpakjian, S. and Schmid, S.R. (2006), "Manufacturing Engineering and Technology" (fifth edition), *Pearson Education, Inc.*

26. Kleszczynski, S., Joschka, Z. J., Sehrt, J. T. (2012), "Error detection in laser beam melting systems by high resolution imaging", In *Proceedings of the 23rd Annual International Solid Freeform Fabrication Symposium - An Additive Manufacturing Conference*, SFF 2012.

27. Matlab. Image Processing Toolbox™ (2018), "User's Guide. Matlab R2018b", *MathWorks.*

28. Mohamed, O. A., Masood, S. H., Bhowmik, J. L. (2016), "Mathematical modeling and FDM process parameters optimization using response surface methodology based on Q-optimal design", *Applied Mathematical Modelling*, Vol. 40 No. 23-24, pp. 10052-10073.

29. Pandey, P. M., Reddy, N. V., Dhande, S. G. (2003), "Real time adaptive slicing for fused deposition modelling", *International Journal of Machine Tools and Manufacture*, Vol. 43 No. 1, pp. 61-71.

30. Popescu, D., Laptoiu, D., Marinescu, R., Botezatu, I. (2018), "Design and 3D printing customized guides for orthopaedic surgery–lessons learned", *Rapid Prototyping Journal*, Vol. 24 No. 5, pp. 901-913.

31. Prakash, K. S., Nancharaih, T., Rao, V. S. (2018), "Additive Manufacturing Techniques in Manufacturing-An Overview", *Materials Today: Proceedings*, Vol. 5 No. 2, pp. 3873-3882.

32. Sher, D. (2018), "Siemens achieves breakthrough with 3D printed gas turbine component", available at: https://www.3dprintingmedia.network/siemens-achieves-breakthrough-3d-printed-gas-turbine-component/ (accessed 14 November 2018).

33. Sood, A. K., Chaturvedi, V., Datta, S., Mahapatra, S. S. (2011), "Optimization of process parameters in fused deposition modeling using weighted principal component analysis", *Journal of Advanced Manufacturing Systems*, Vol. 10 No. 2, pp. 241-259.

34. Thomas, D. (2009), "The Development of Design Rules for Selective Laser Melting", *Ph.D. Thesis,* University of Wales Institute, Cardiff.

35. Thompson, M. K., Moroni, G., Vaneker, T., Fadel, G., Campbell, R. I., Gibson, I., Martina, F. (2016), "Design for Additive Manufacturing: Trends, opportunities, considerations, and constraints", *CIRP annals*, Vol. 65 No. 2, pp. 737-760.

36. Tong, K., Joshi, S., Amine Lehtihet, E. (2008), "Error compensation for fused deposition modeling (FDM) machine by correcting slice files", *Rapid Prototyping Journal*, Vol. 14 No. 1, pp. 4-14.

37. Townsend, A., Senin, N., Blunt, L., Leach, R. K., Taylor, J. S. (2016), "Surface texture metrology for metal additive manufacturing: a review", *Precision Engineering*, Vol. 46, pp. 34-47.

38. Tyczynski, P., Siemiatkowski, Z., Rucki, M. (2018), "Analysis of the drill base body fabricated with Additive Manufacturing technology", *euspen's 18th International Conference & Exhibition, Venice, IT, June 2018.*

39. Vaezi, M., Safaeian, D., Chua, C. K. (2011), "Gas turbine blade manufacturing by use of epoxy resin tooling and silicone rubber molding techniques", *Rapid Prototyping Journal*, Vol. 17 No. 2, pp. 107-115.

40. Vaezi, M., Seitz, H., Yang, S. (2013), "A review on 3D micro-additive manufacturing technologies", *The International Journal of Advanced Manufacturing Technology*, Vol. 67 No. 5-8, pp. 1721-1754.

41. Vayre, B., Vignat, F., Villeneuve, F. (2012), "Designing for additive manufacturing", *Procedia CIrP*, Vol. 3, pp. 632-637.

42. VDI 3405 (2014-12), "Additive manufacturing processes, rapid manufacturing - Basics, definitions, processes".

43. Wang, A., Song, S., Huang, Q., Tsung, F. (2017), "In-plane shape-deviation modeling and compensation for fused deposition modeling processes", *IEEE Transactions on Automation Science and Engineering*, Vol. 14 No. 2, pp. 968-976.

44. Wu, H., Wang, Y., Yu, Z. (2016), "In situ monitoring of FDM machine condition via acoustic emission", *The International Journal of Advanced Manufacturing Technology*, Vol. 84 No. 5-8, pp. 1483-1495.

45. Xu, G., Zhao, W., Tang, Y., Lu, B. (2007), "Development of a high–resolution rapid prototyping system for small size objects", *The International Journal of Advanced Manufacturing Technology*, Vol. 31 No. 9-10, pp. 941-947.

46. Xu, L., Huang, Q., Sabbaghi, A., Dasgupta, T. (2013), "Shape deviation modeling for dimensional quality control in additive manufacturing", In *ASME 2013 International Mechanical Engineering Congress and Exposition* (pp. V02AT02A018-V02AT02A018). American Society of Mechanical Engineers.

47. Yoon, J., He, D., Van Hecke, B. (2014), "A PHM approach to additive manufacturing equipment health monitoring, fault diagnosis, and quality control", In *Proceedings of the Prognostics and Health Management Society Conference, Fort Worth, TX, USA,* Vol. 29, pp. 1-9.

48. Zha, W., Anand, S. (2015), "Geometric approaches to input file modification for part quality improvement in additive manufacturing", *Journal of Manufacturing Processes*, Vol. 20, pp. 465-477.

49. Zieliński, D. (2017), "Application of Rapid Prototyping techniques for micro-holes manufacturing", *Master Thesis*, Gdansk University of Technology, Gdansk.

50. Zieliński, D. (2018-03), "3D printing of polymers on an industrial scale in SLS technology (in Polish)", available at: https://drukarki3d.pl/aktualnosci/druk-3d-czesci-z-tworzyw-sztucznych-na-skale-przemyslowa/ (accessed 7 February 2019).

51. Zieliński, D. (2018-09), "Liebherr – the first metal 3D printed main hydraulic element of the flight control system used in the Airbus A380 aircraft (in Polish)", available at: https://drukarki3d.pl/wdrozenia/liebherr/ (accessed 7 February 2019).
52. Zieliński, D. (2018-10), "Topology optimisation of an aerospace components (in Polish)", available at: https://staleo.pl/z-kraju-i-ze-swiata/technologie/3353/optymalizacja-topologiczna-czesci-lotniczych (accessed 7 February 2019).
53. Zur Jacobsmühlen, J., Kleszczynski, S., Schneider, D., Witt, G. (2013), "High resolution imaging for inspection of laser beam melting systems", In *2013 IEEE International Instrumentation and Measurement Technology Conference (I2MTC)*. IEEE, pp. 707-712.

Figure 1

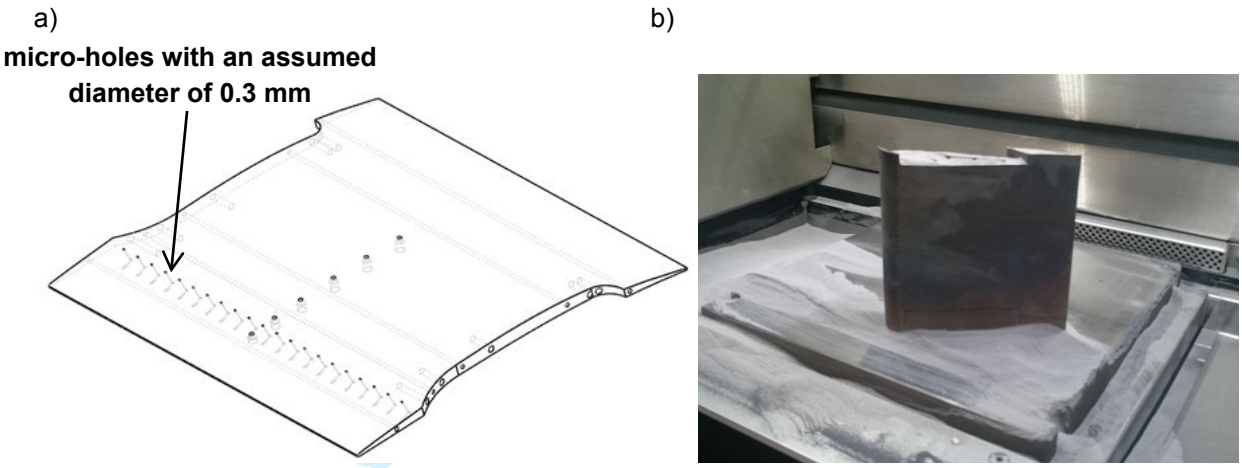

Figure 1: Gas turbine blade: a) CAD model with 0.3 mm diameter holes, b) the working chamber of the 3D printer with a manufactured part (Zieliński, 2017)

"A pilot study to assess an in-process inspection method for small diameter holes produced by Direct Metal Laser Sintering"

Figure 2

a) b)

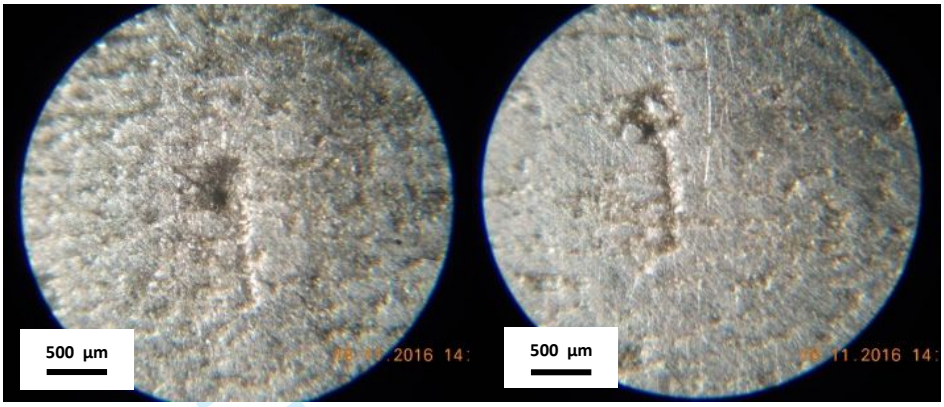

Figure 2. Spots of forming the micro-holes of 0.3 mm diameter on blade surface: a) a nucleus of micro-hole, b) a tear-off on material surface (Deja *et al.*, 2018)

"A pilot study to assess an in-process inspection method for small diameter holes produced by Direct Metal Laser Sintering"

Figure 3

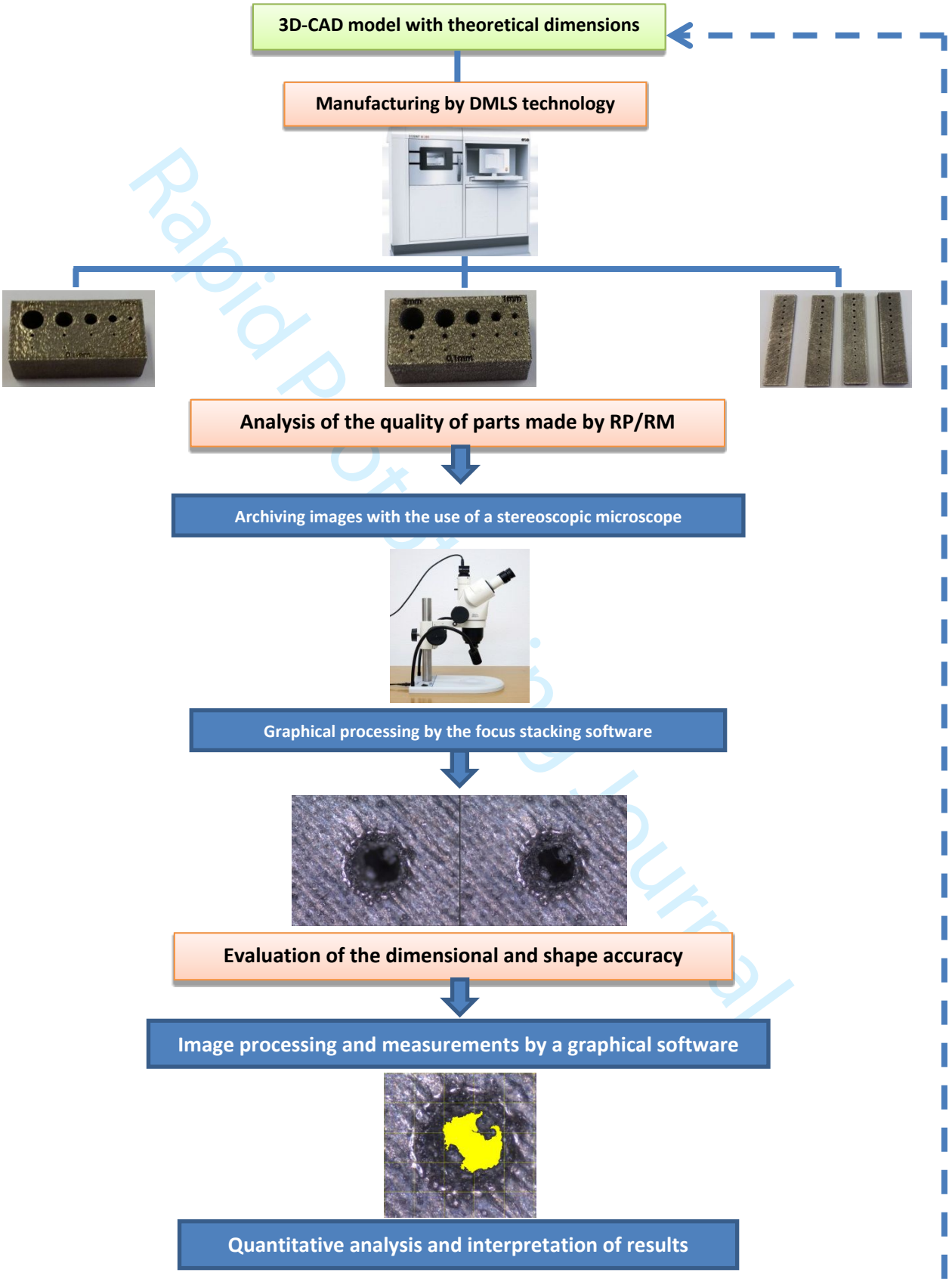
3D-CAD model with theoretical dimensions
Manufacturing by DMLS technology
Analysis of the quality of parts made by RP/RM
Archiving images with the use of a stereoscopic microscope
Graphical processing by the focus stacking software
Evaluation of the dimensional and shape accuracy
Image processing and measurements by a graphical software
Quantitative analysis and interpretation of results

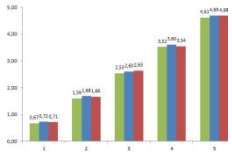

Determination of the dimensions in a CAD model for obtaining the required diameters in a real part

Figure 3. Scheme of the adopted research methodology

"A pilot study to assess an in-process inspection method for small diameter holes produced by Direct Metal Laser Sintering"

Figure 4

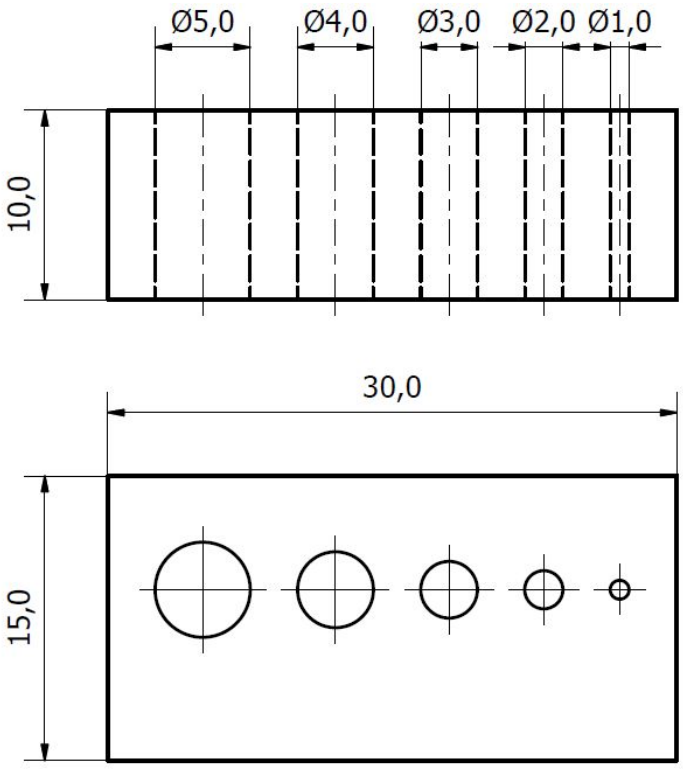

Figure 4. Drawing of a test sample with holes of diameters ranging from 1 mm to 5 mm

"A pilot study to assess an in-process inspection method for small diameter holes produced by Direct Metal Laser Sintering"

Figure 5

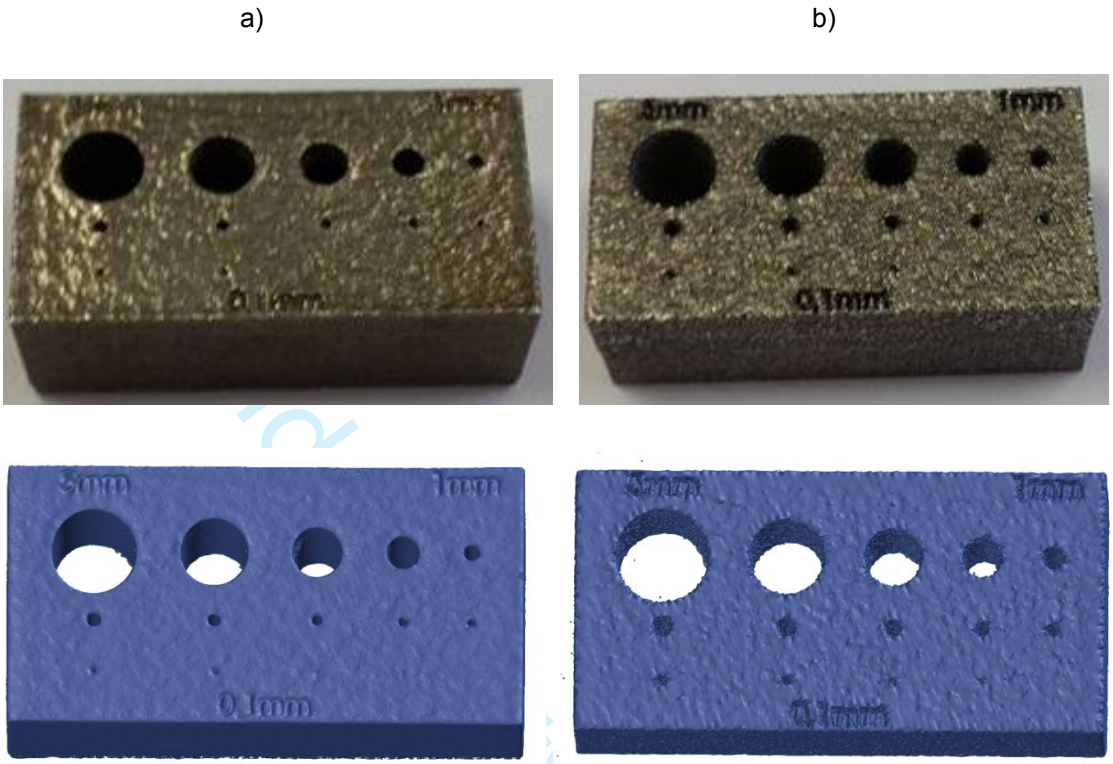

Figure 5. Samples made of EOS MaragingSteel MS1 (a) and aluminium alloy EOS Aluminium (b) with relevant digital models obtained by a computer tomography

"A pilot study to assess an in-process inspection method for small diameter holes produced by Direct Metal Laser Sintering"

Figure 6

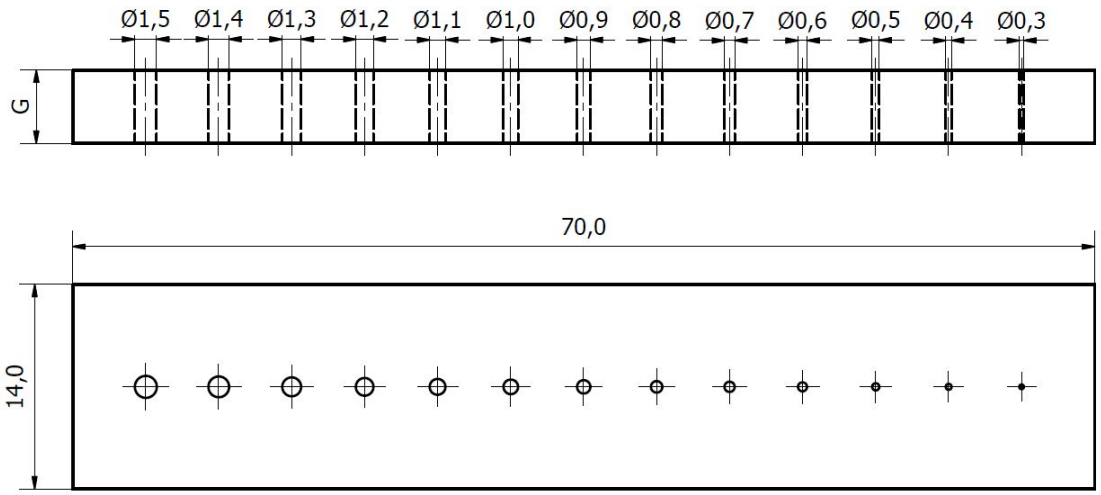

Figure 6. Straight through holes designed in a sample of a variable thickness: G = 1 mm, 2 mm, 4 mm and 5 mm

"A pilot study to assess an in-process inspection method for small diameter holes produced by Direct Metal Laser Sintering"

Figure 7

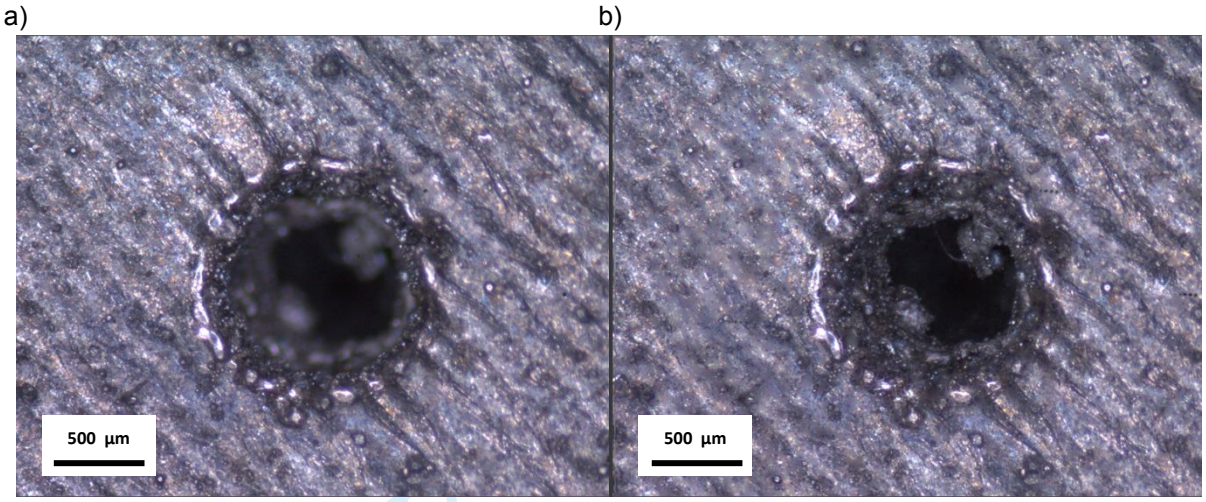

Figure 7: Images of the hole before (a) and after (b) a focus stacking

"A pilot study to assess an in-process inspection method for small diameter holes produced by Direct Metal Laser Sintering"

Figure 8

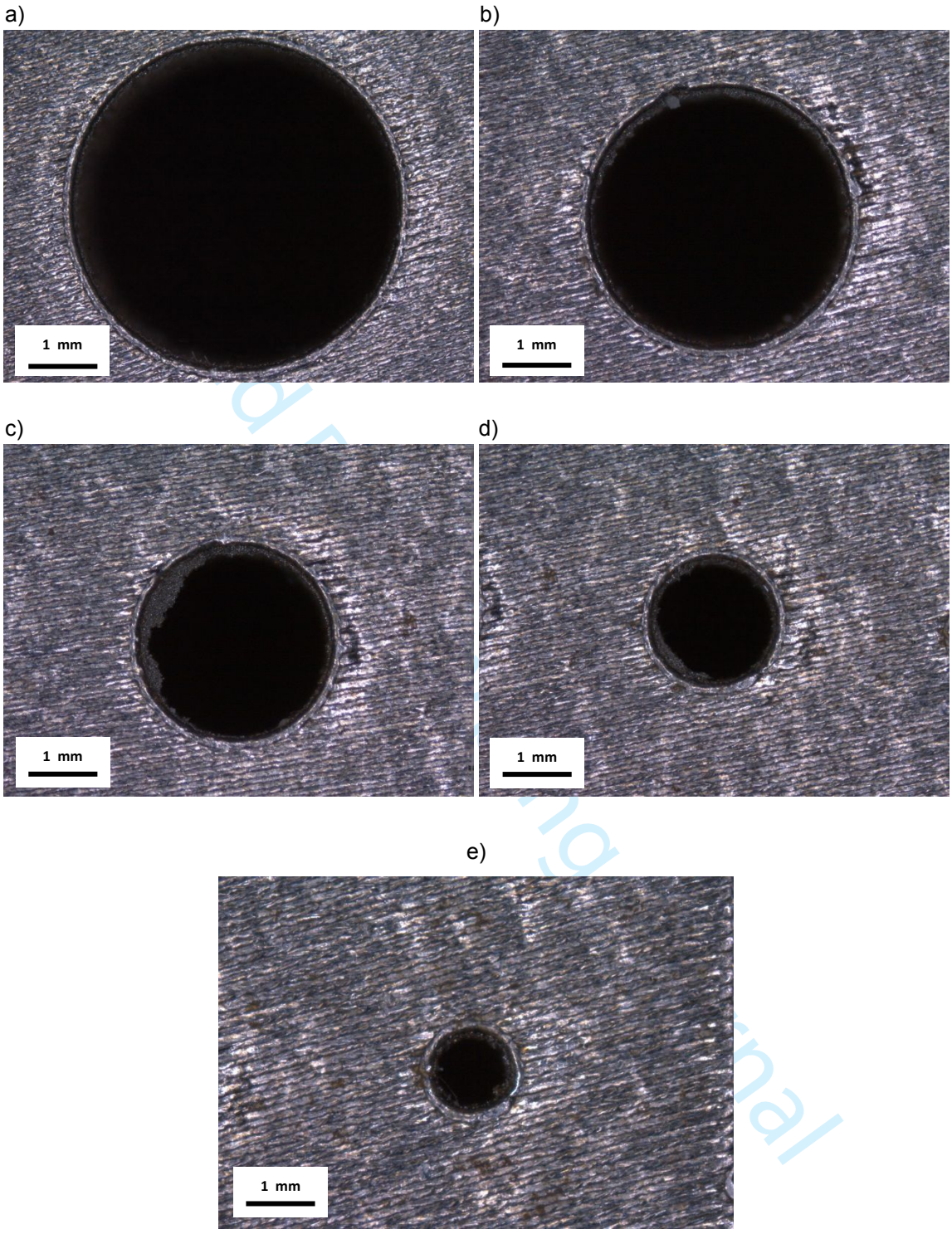

Figure 8. Test sample made of EOS MaragingSteel MS1 with holes of assumed diameters of: a) 5 mm, b) 4 mm, c) 3 mm, d) 2 mm and e) 1 mm

"A pilot study to assess an in-process inspection method for small diameter holes produced by Direct Metal Laser Sintering"

Figure 9

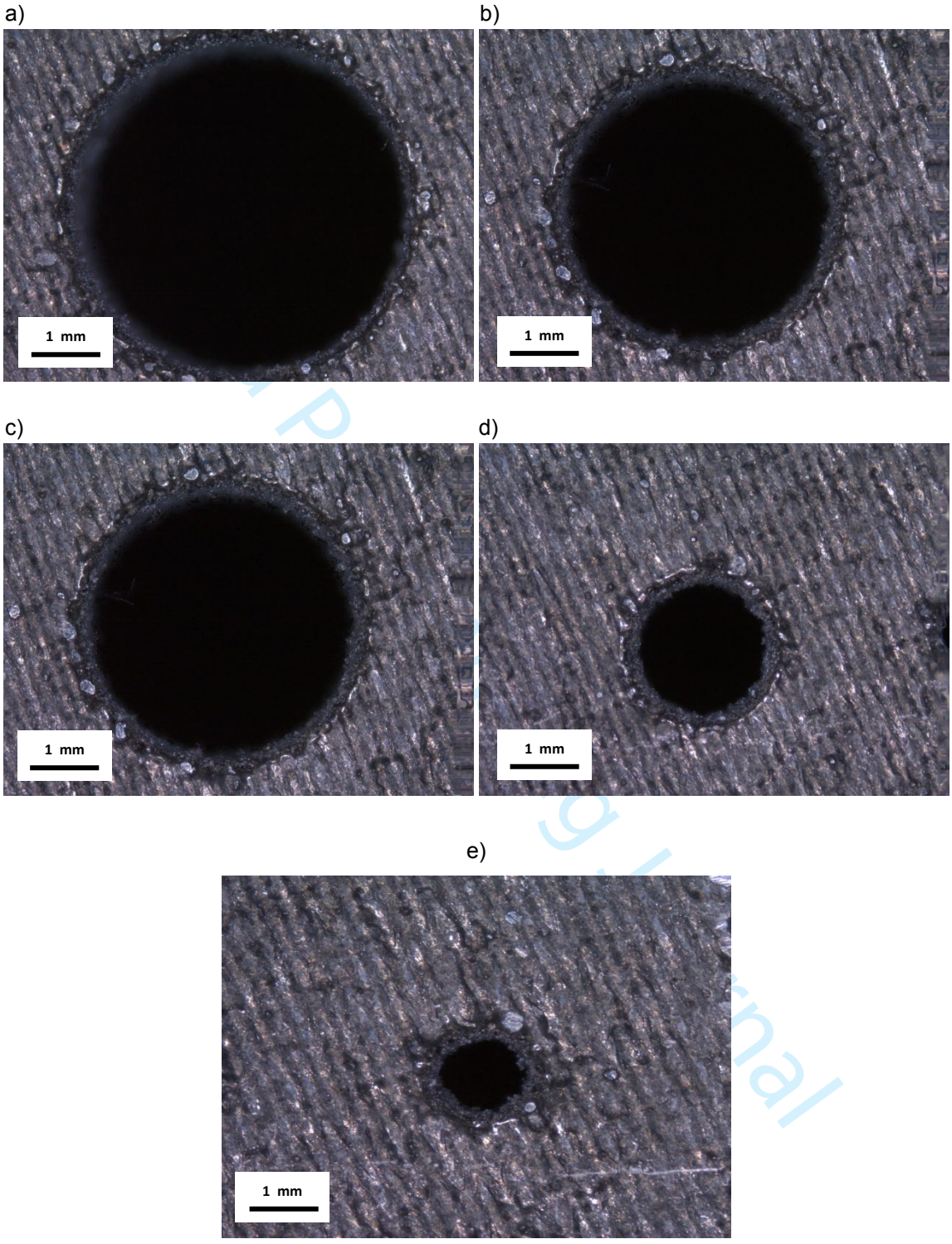

Figure 9. Test sample made of EOS Aluminium AlSi10Mg with holes of assumed diameters of: a) 5 mm, b) 4 mm, c) 3 mm, d) 2 mm and e) 1 mm

"A pilot study to assess an in-process inspection method for small diameter holes produced by Direct Metal Laser Sintering"

Figure 10

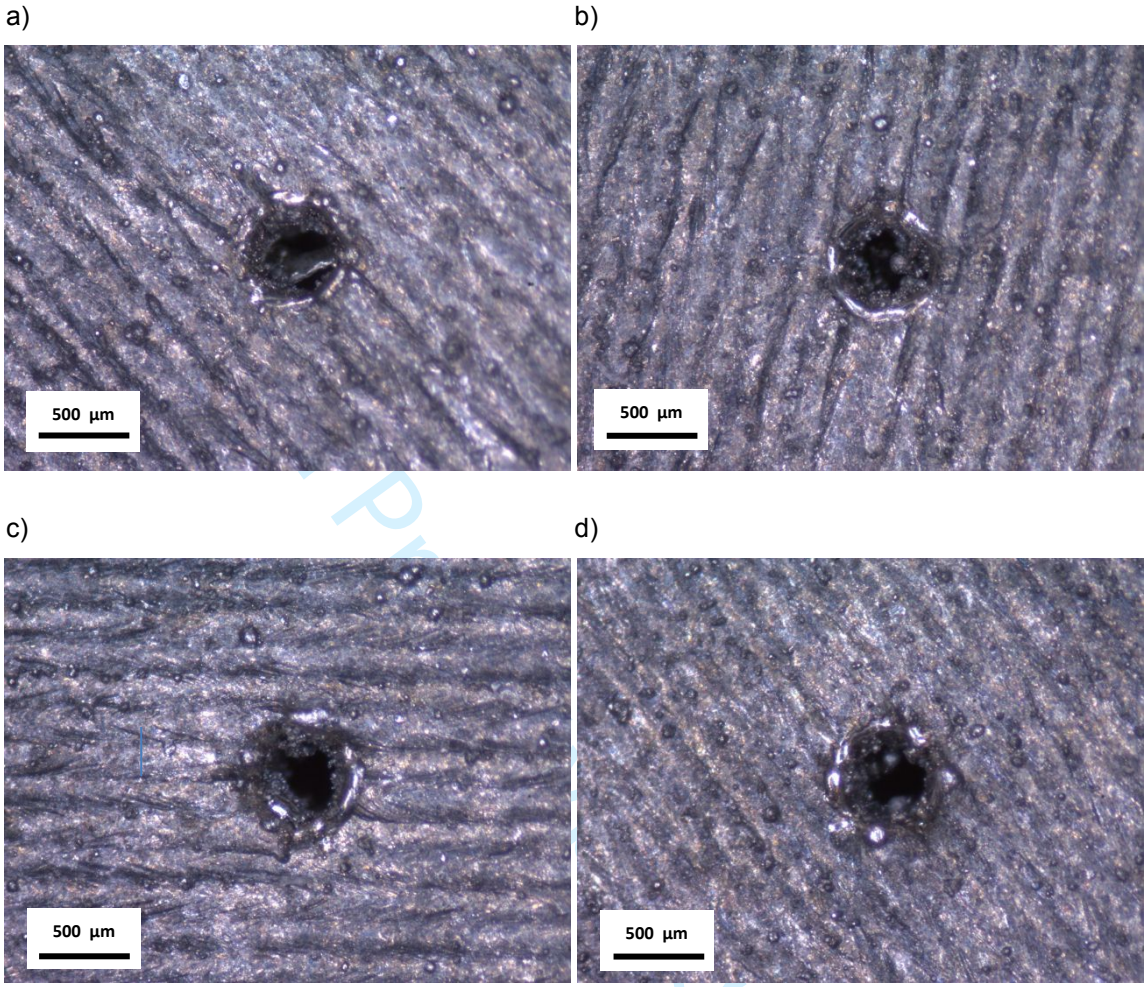

Figure 10. Test samples made of EOS Aluminium AlSi10Mg material with holes of an assumed 0.3 mm diameter and a variable thickness: a) 1 mm, b) 2 mm, c) 4 mm and d) 5 mm

"A pilot study to assess an in-process inspection method for small diameter holes produced by Direct Metal Laser Sintering"

Figure 11

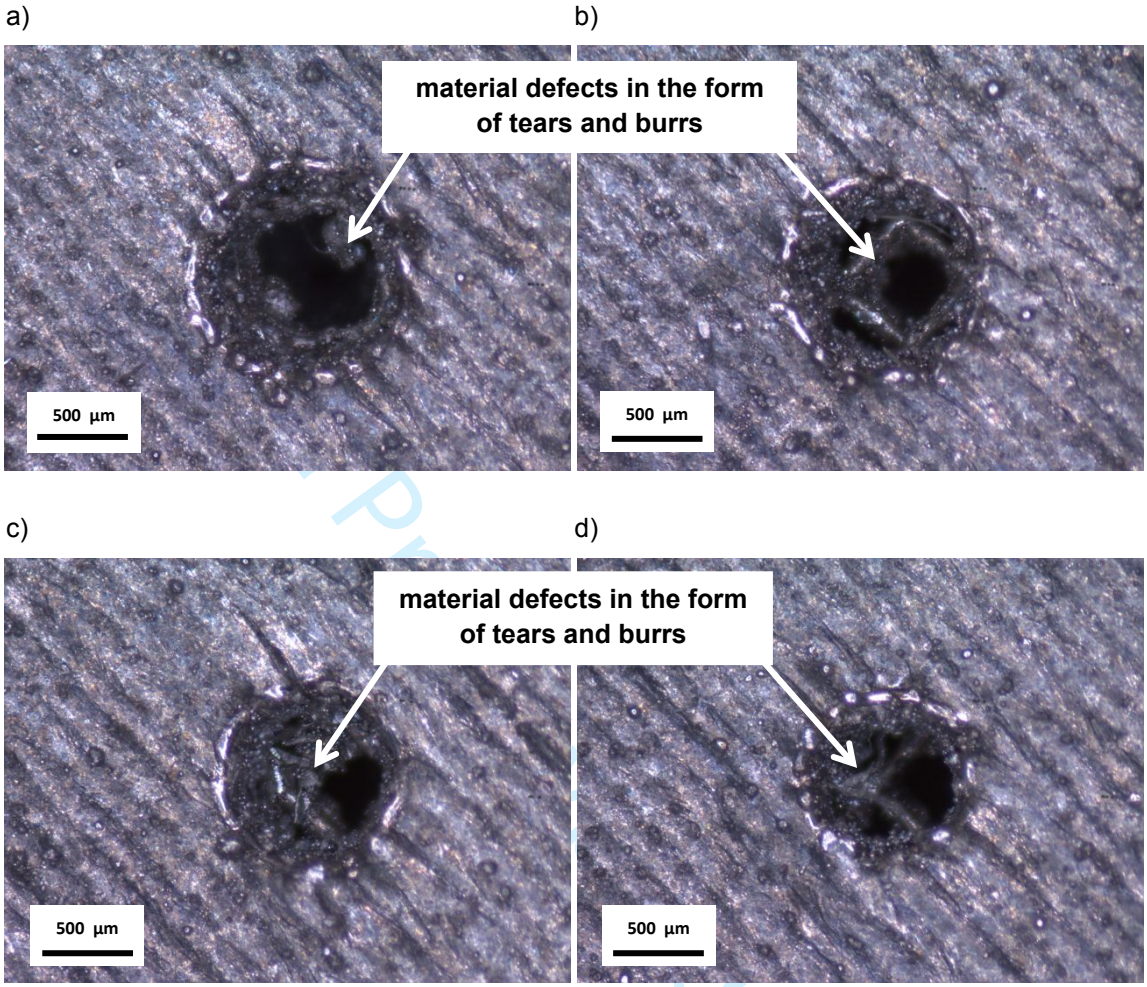

Figure 11. The 1 mm thick test sample manufactured from EOS Aluminium AlSi10Mg material with holes of assumed diameters: a) 1 mm, b) 0.9 mm, c) 0.8 mm and d) 0.7 mm

"A pilot study to assess an in-process inspection method for small diameter holes produced by Direct Metal Laser Sintering"

Figure 12

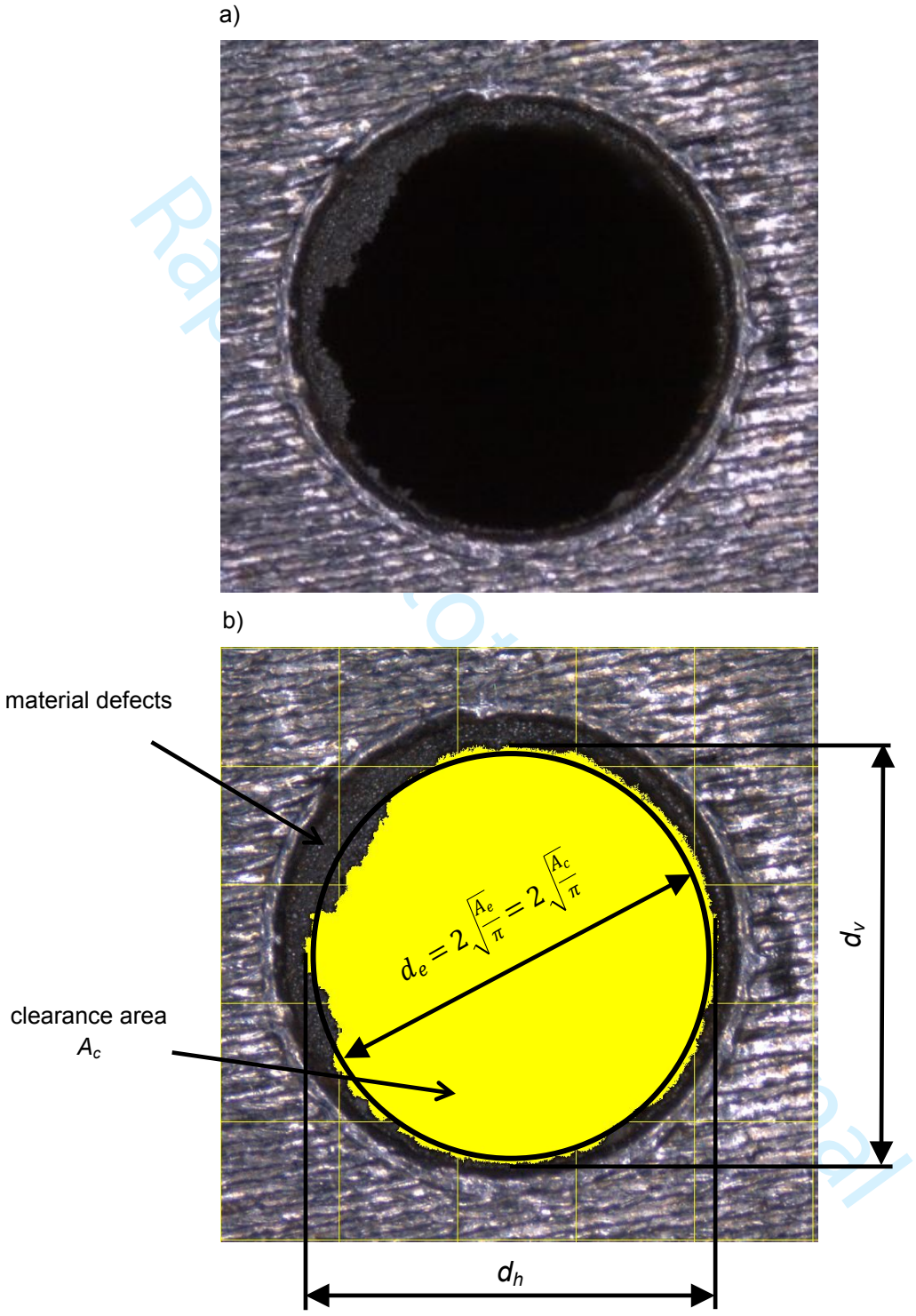

Figure 12. The sample made of MS1 material with the hole of an assumed diameter d_t = 3 mm: a) top view of the hole before the measurements, b) top view of the hole after the determination of its clearance area and Feret's diameters: horizontal d_h and vertical d_v; d_e – equivalent hole diameter

“A pilot study to assess an in-process inspection method for small diameter holes produced by Direct Metal Laser Sintering”

Figure 13

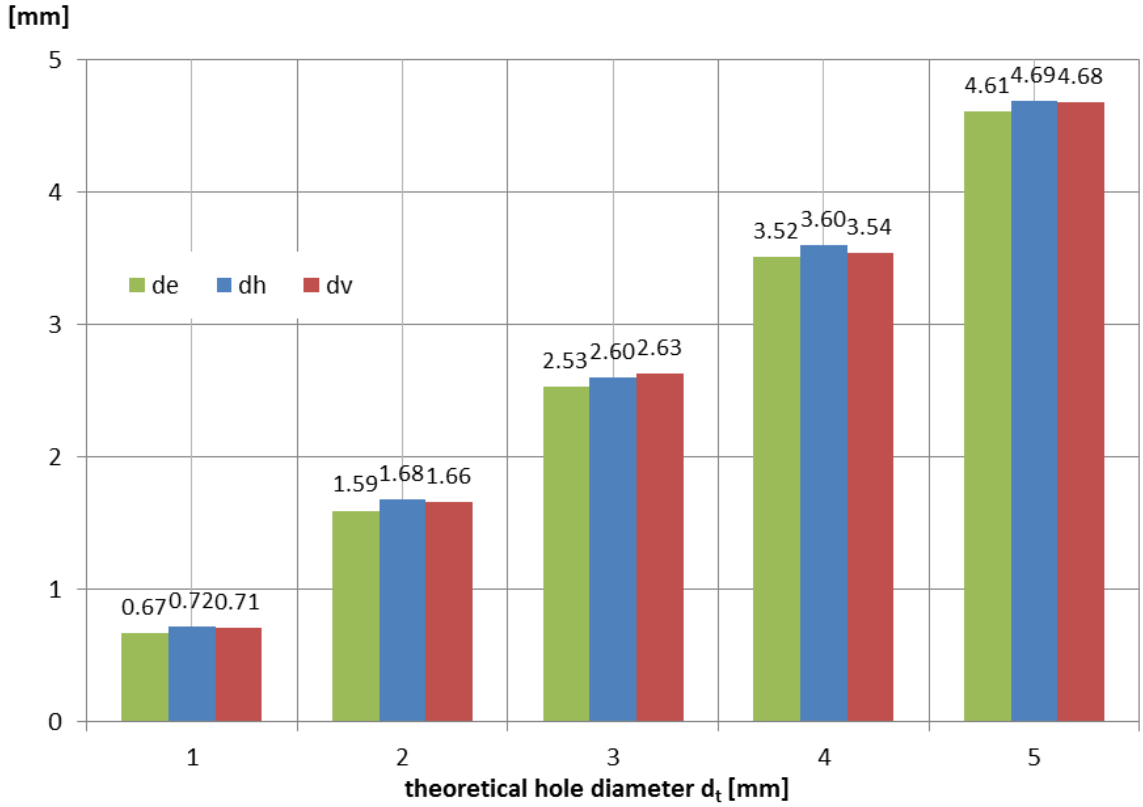

Figure 13. Hole diameters d_e, d_v, d_h determined for a 10 mm thick test sample made of MS1 material

"A pilot study to assess an in-process inspection method for small diameter holes produced by Direct Metal Laser Sintering"

Figure 14

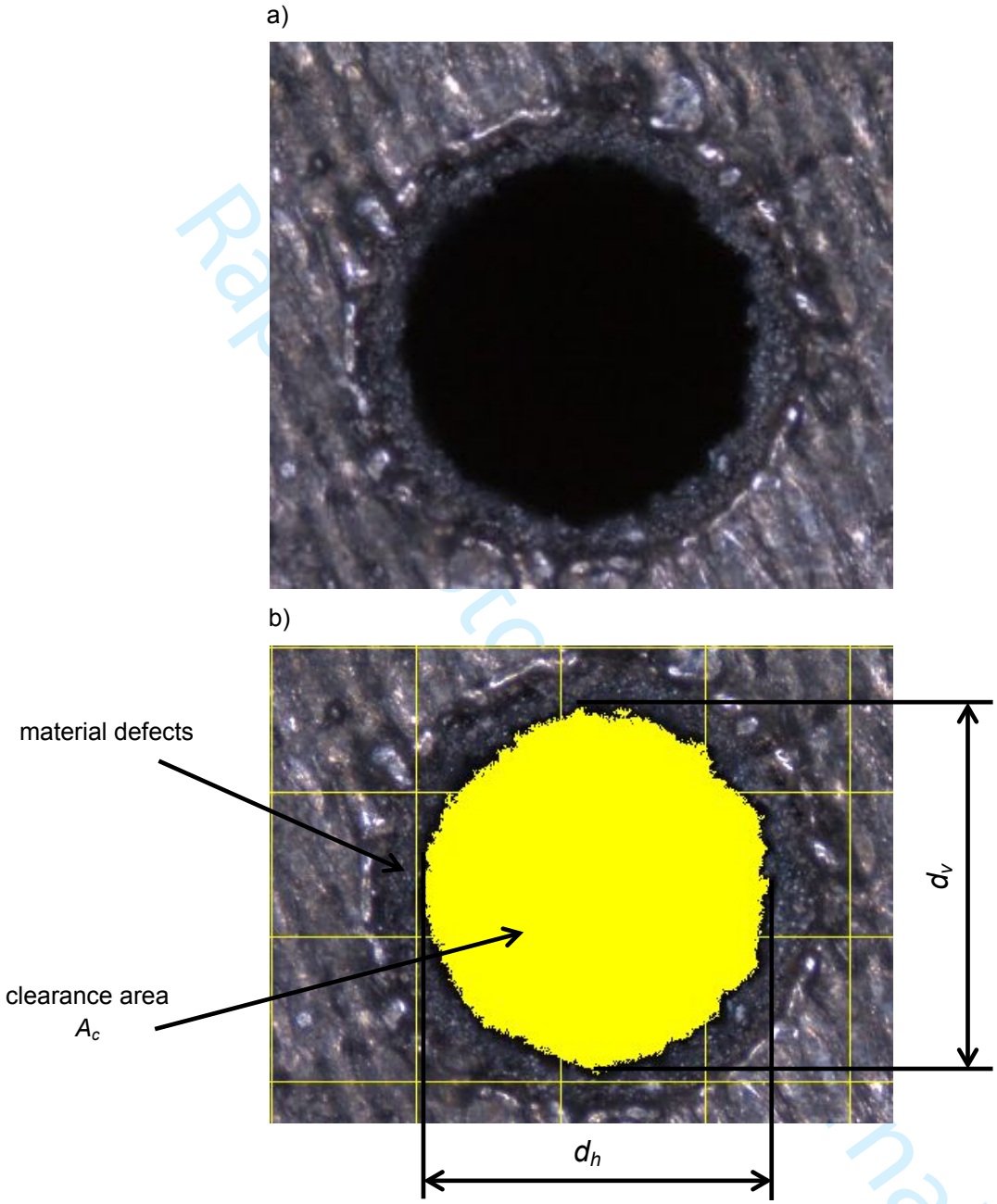

Figure. 14. The sample made of aluminium alloy with the hole of an assumed diameter d_t = 2 mm: a) top view of the hole before the measurements, b) top view of the hole after the determination of its clearance and Feret's diameters: horizontal d_h and vertical d_v

"A pilot study to assess an in-process inspection method for small diameter holes produced by Direct Metal Laser Sintering"

Figure 15

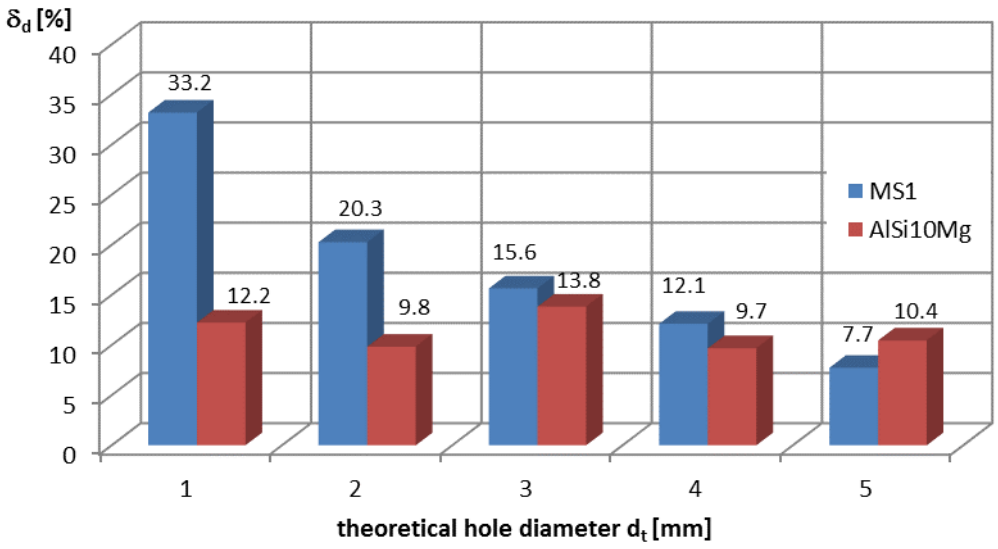

Figure 15. Relative errors of the hole diameter for a 10 mm thick test sample

"A pilot study to assess an in-process inspection method for small diameter holes produced by Direct Metal Laser Sintering"

Figure 16

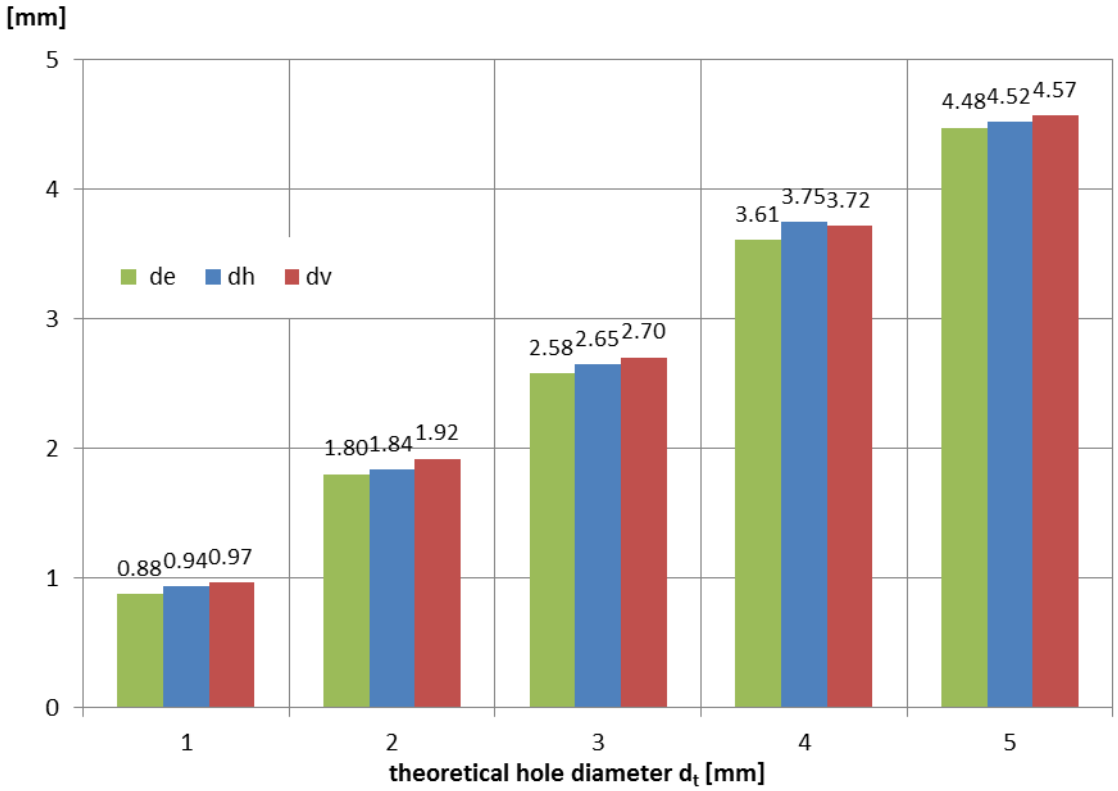

Figure 16. Hole diameters d_e, d_v, d_h determined for a 10 mm thick test sample made of EOS Aluminium AlSi10Mg material

"A pilot study to assess an in-process inspection method for small diameter holes produced by Direct Metal Laser Sintering"

Figure 17

a)

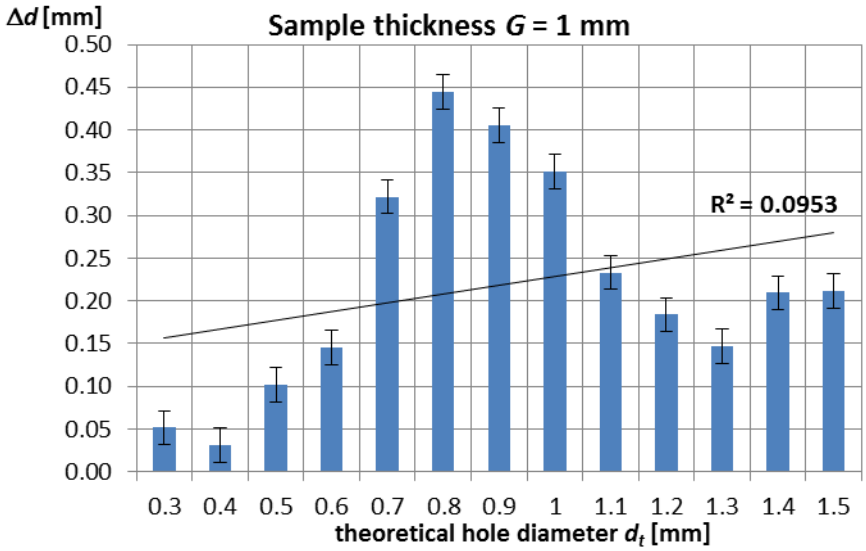
Δd [mm]
Sample thickness G = 1 mm
0.50
0.45
0.40
0.35
0.30
0.25
0.20
0.15
0.10
0.05
0.00
R² = 0.0953
0.3 0.4 0.5 0.6 0.7 0.8 0.9 1 1.1 1.2 1.3 1.4 1.5
theoretical hole diameter d_t [mm]

b)

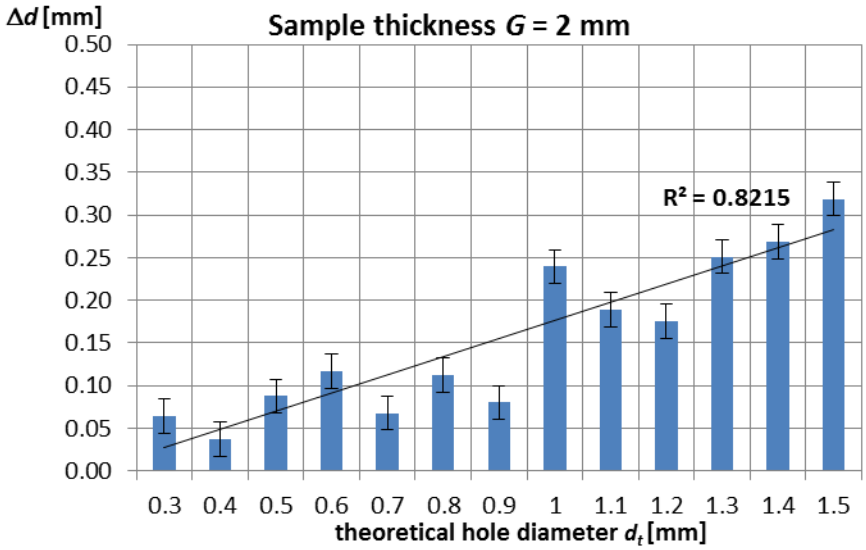
Δd [mm]
Sample thickness G = 2 mm
0.50
0.45
0.40
0.35
0.30
0.25
0.20
0.15
0.10
0.05
0.00
R² = 0.8215
0.3 0.4 0.5 0.6 0.7 0.8 0.9 1 1.1 1.2 1.3 1.4 1.5
theoretical hole diameter d_t [mm]

c)

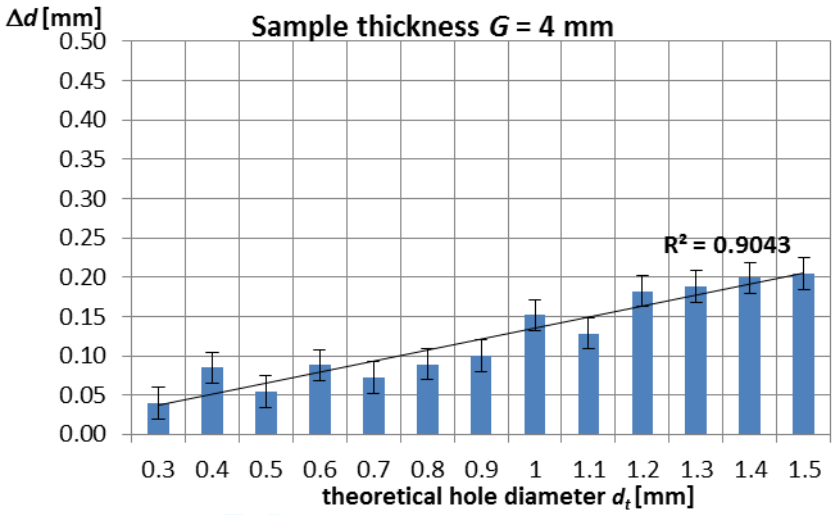

d)

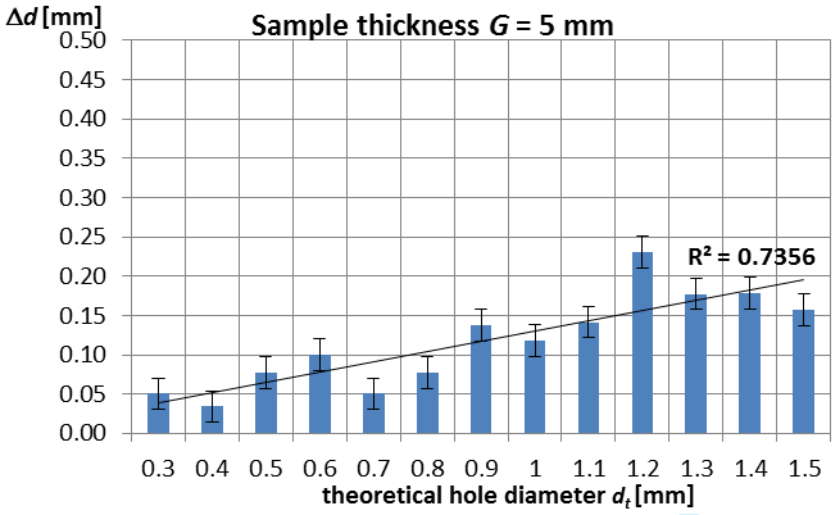

Figure 17. Absolute errors of the hole diameter for a test sample made of EOS Aluminium AlSi10Mg material for the thickness *G* of: a) 1 mm, b) 2 mm, c) 4 mm, and d) 5 mm

Figure 18

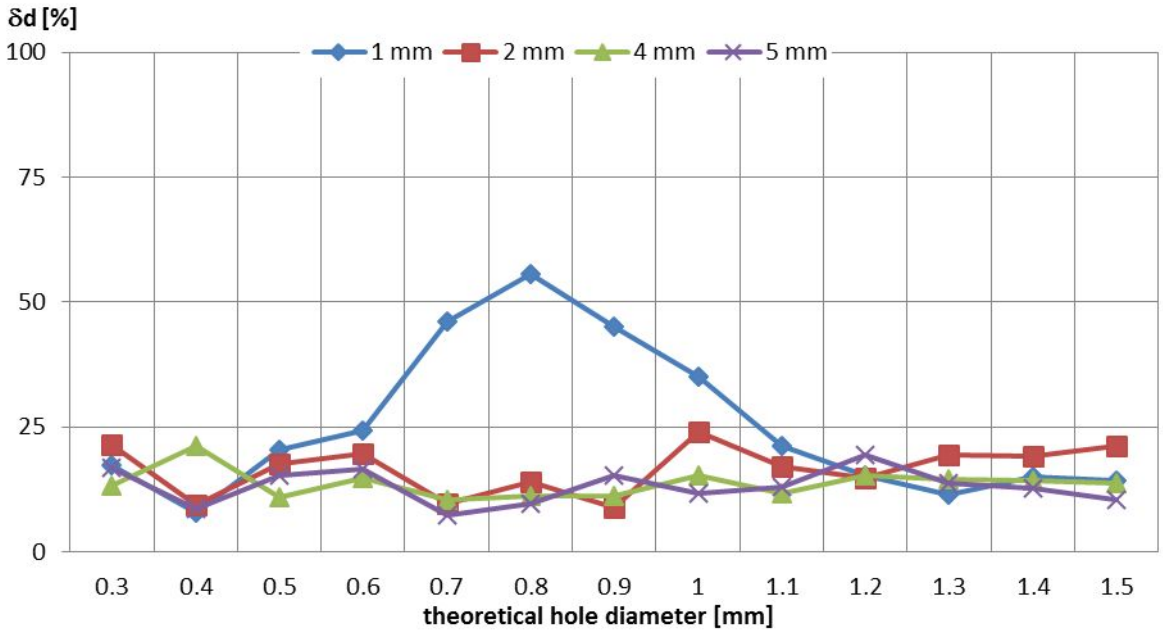

Figure 18. Relative errors of the theoretical hole diameter d_t for a test sample of a different thickness, made of EOS Aluminium AlSi10Mg material

"A pilot study to assess an in-process inspection method for small diameter holes produced by Direct Metal Laser Sintering"

Figure 19

a)

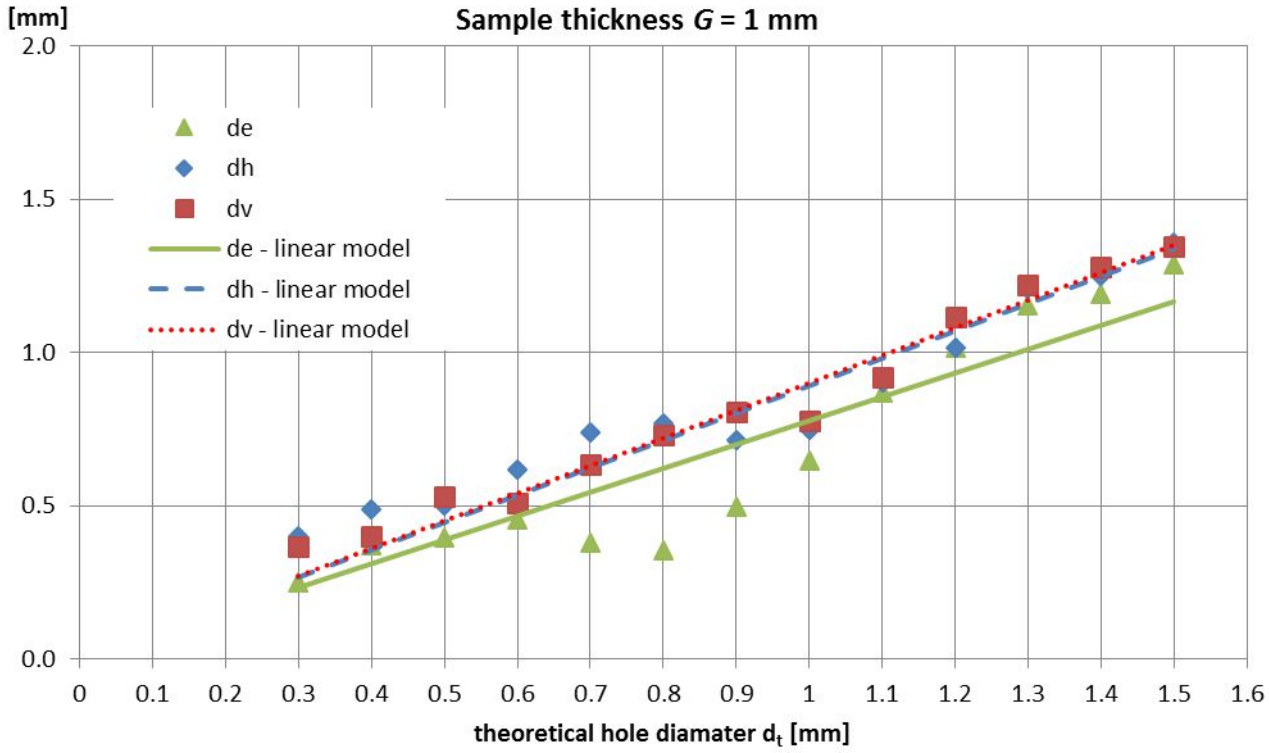
[mm]
Sample thickness G = 1 mm
2.0
1.5
1.0
0.5
0.0
de
dh
dv
de - linear model
dh - linear model
dv - linear model
0
0.1
0.2
0.3
0.4
0.5
0.6
0.7
0.8
0.9
1
1.1
1.2
1.3
1.4
1.5
1.6
theoretical hole diamater d_t [mm]

b)

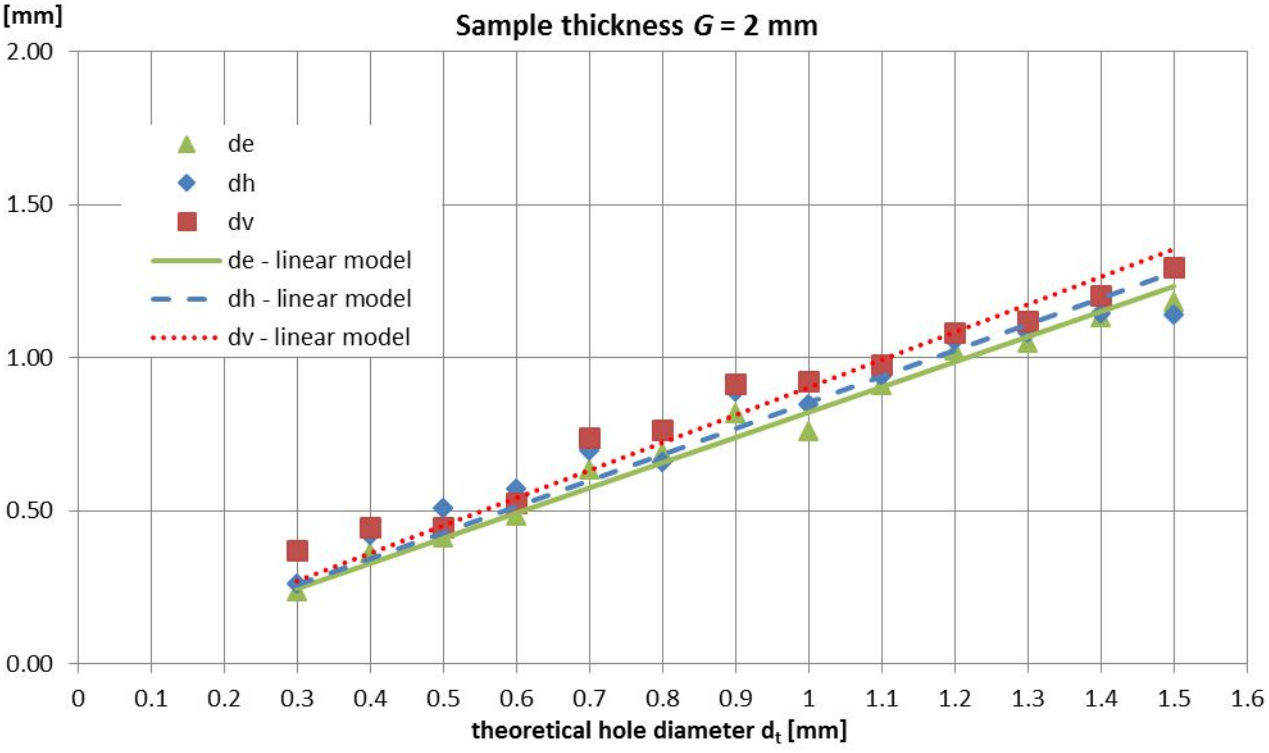
[mm]
Sample thickness G = 2 mm
2.00
1.50
1.00
0.50
0.00
de
dh
dv
de - linear model
dh - linear model
dv - linear model
0
0.1
0.2
0.3
0.4
0.5
0.6
0.7
0.8
0.9
1
1.1
1.2
1.3
1.4
1.5
1.6
theoretical hole diameter d_t [mm]

c)

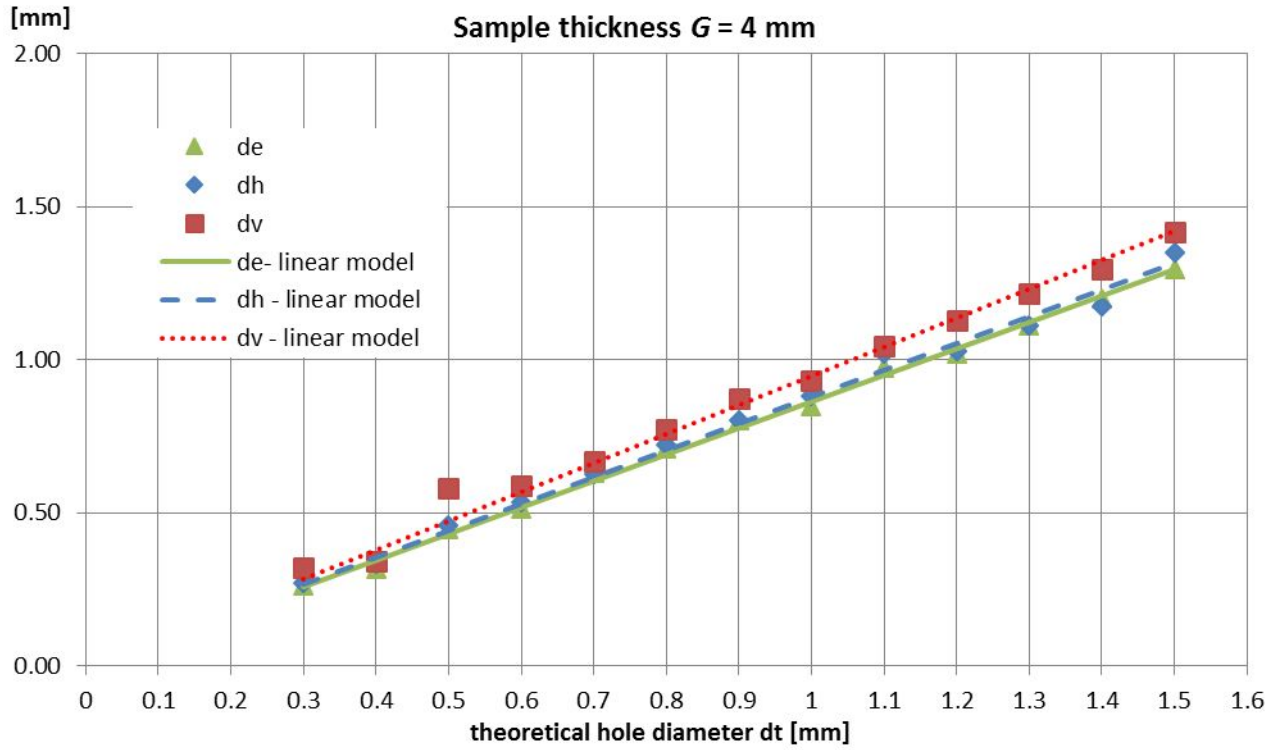

d)

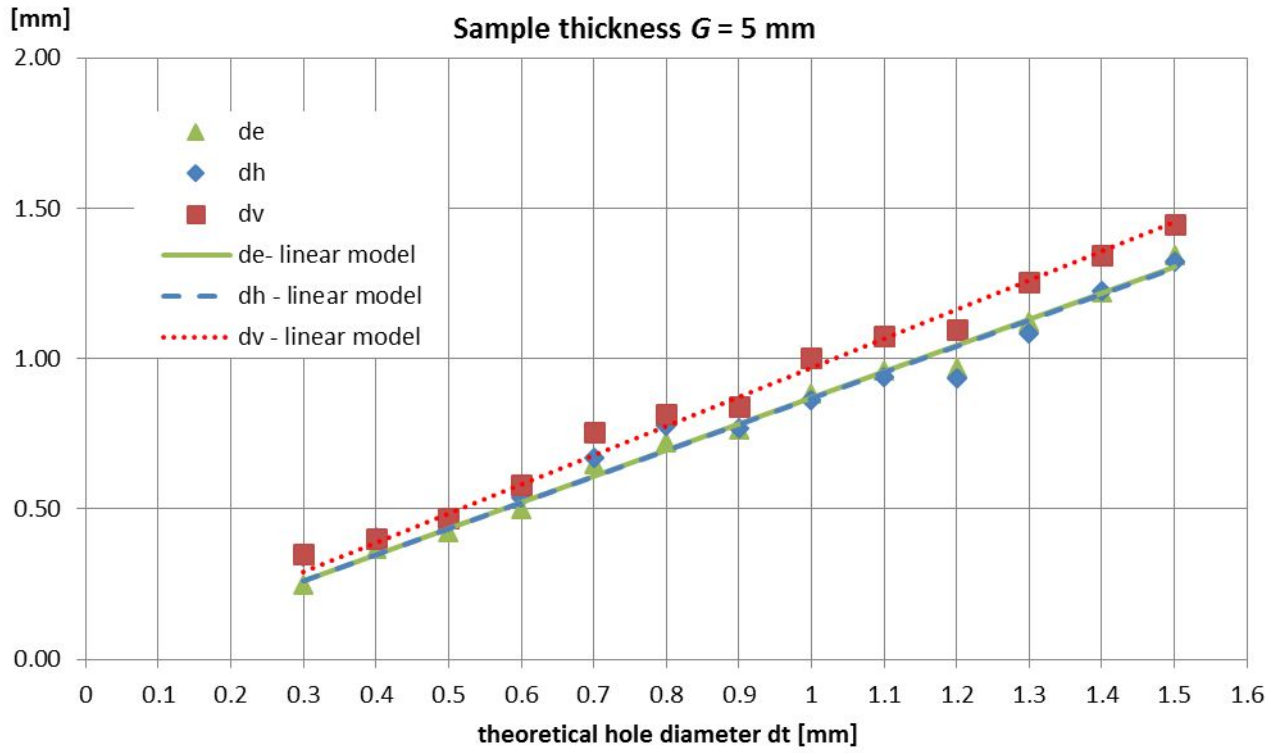

Figure 19. Linear fitting of analysed hole diameters for samples made of EOS Aluminium AlSi10Mg material for a thickness *G* of: a) 1 mm, b) 2 mm, c) 4 mm, and d) 5 mm

"A pilot study to assess an in-process inspection method for small diameter holes produced by Direct Metal Laser Sintering"

Figure 20

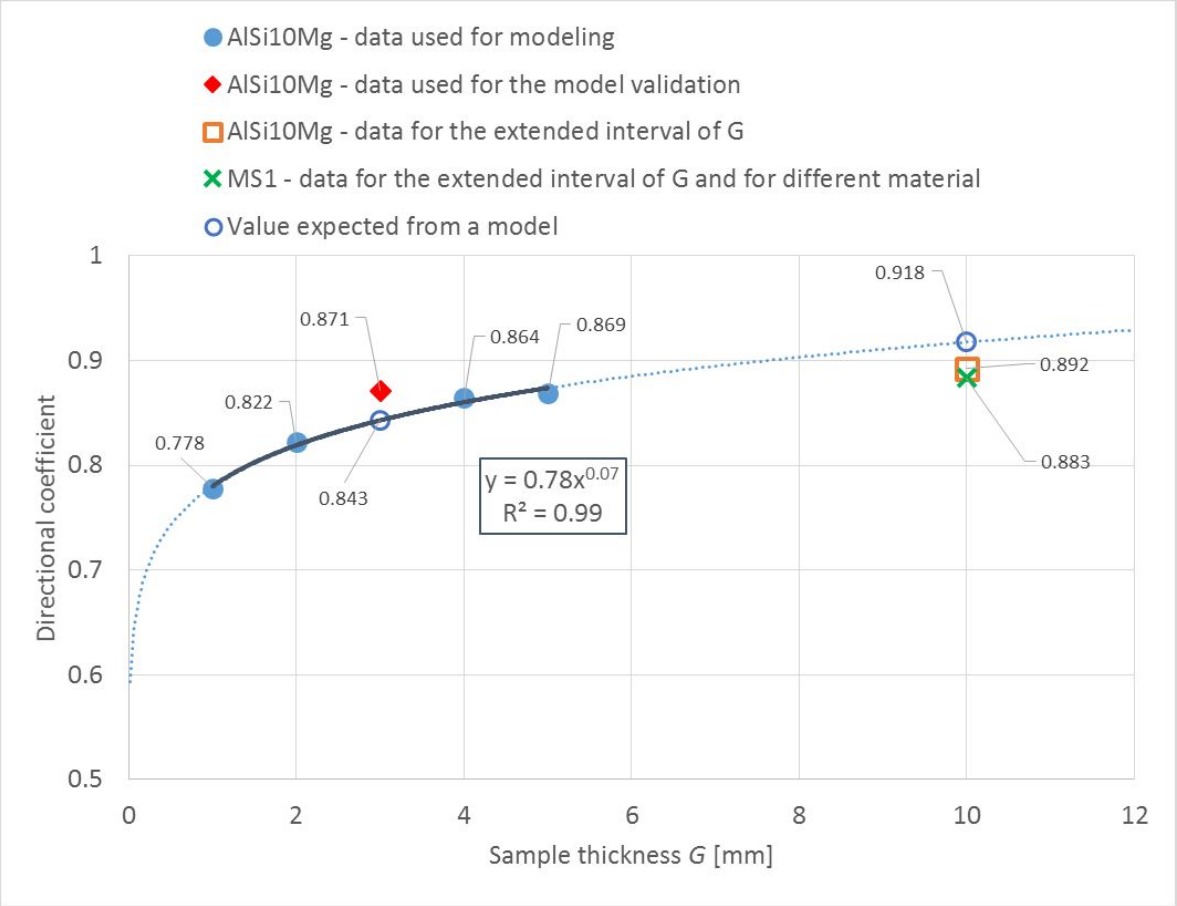

Figure 20. The relationship between a sample thickness (hole length) G and the directional coefficient of a linear function for calculating the equivalent hole diameter d_e; —— the coefficient $\hat{a}$ for the intervals of G and d_t used for modelling, $G \in [1, 5]$ and $d_t \in [0.3, 1.5]$; ····· the coefficient $\hat{a}$ for the extended interval of G and d_t

"A pilot study to assess an in-process inspection method for small diameter holes produced by Direct Metal Laser Sintering"

Figure 21

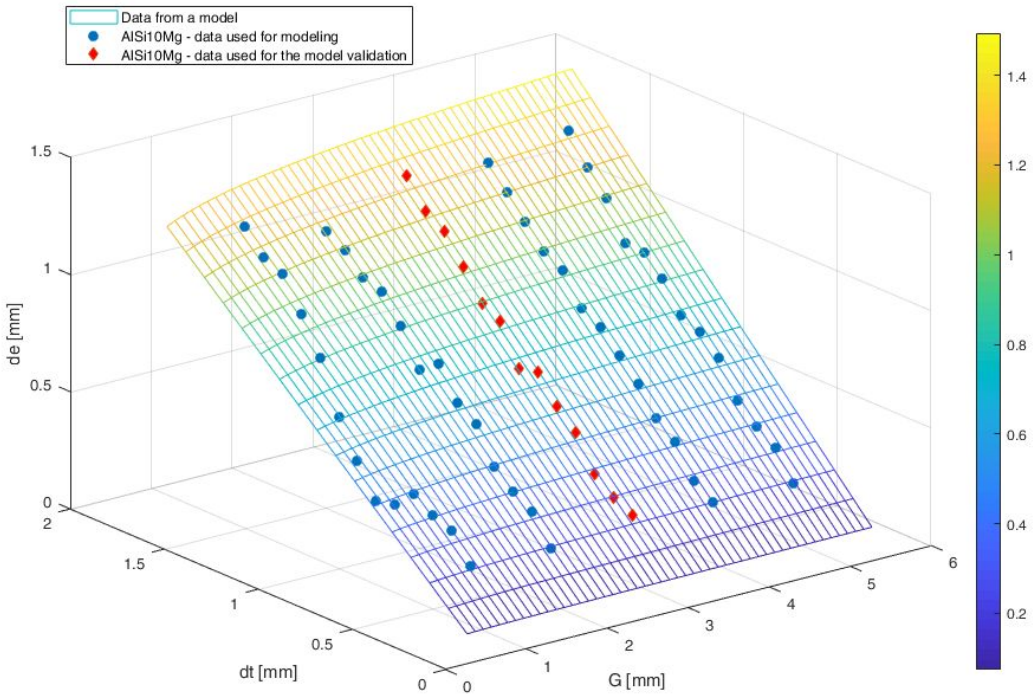

Figure 21. Obtained and predicted equivalent hole diameter d_e for a sample thickness $G \in [1, 5]$ and a theoretical hole diameter $d_t \in [0.3, 1.5]$

"A pilot study to assess an in-process inspection method for small diameter holes produced by Direct Metal Laser Sintering"

Figure 22

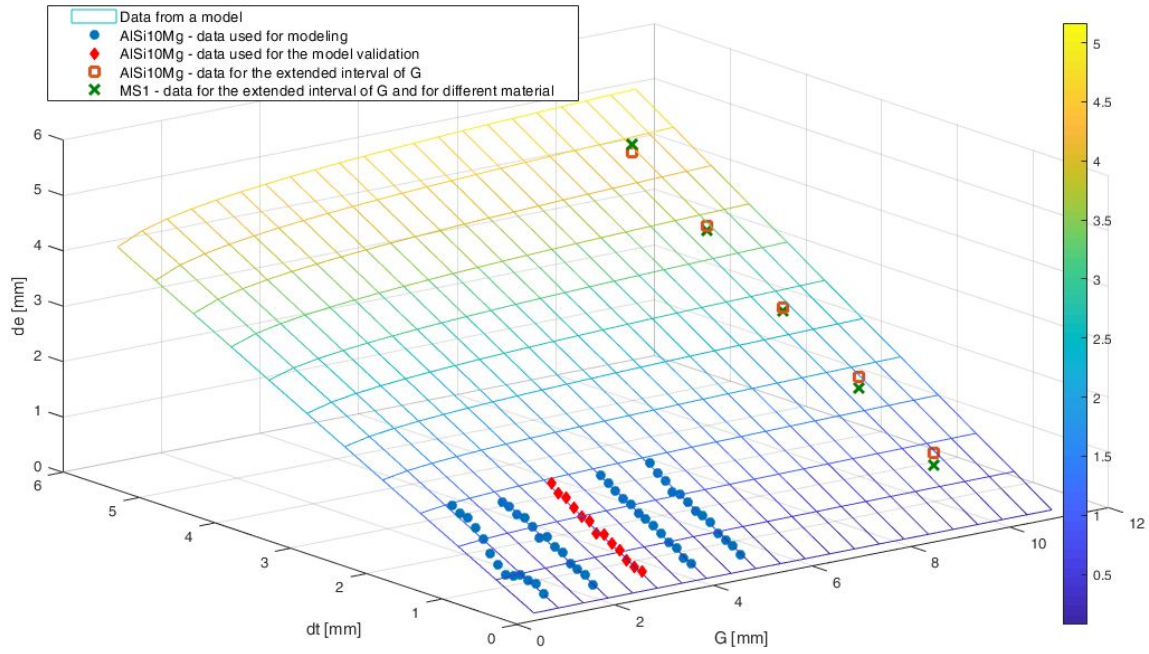

Figure 22. Obtained and predicted equivalent hole diameter d_e for the extended intervals of a sample thickness $G \in [1, 10]$ and a theoretical hole diameter $d_t \in [0.3, 5]$

"A pilot study to assess an in-process inspection method for small diameter holes produced by Direct Metal Laser Sintering"

Table 1

Table 1. Most popular 3D printing technologies with the characteristics of the construction of the physical model and the source of energy generated for the incremental process.

3D printing technology		The way of building a physical model	Source of energy generated for the process
Symbol of the method	**Name of the method**		
SLS	Selective Laser Sintering	selective laser sintering of plastic powders	concentrated beam of laser generated rays, usually CO_2
DMLS	Direct Metal Laser Sintering	selective laser melting of metal powders with different melting temperatures (individual metals and their alloys)	laser beam
SLM	Selective Laser Melting	selective laser melting of metal powders with the same melting point (single metals)	laser beam
PJM/MJM	Poly-Jet Modeling/Multi-Jet Modeling	spraying by piezoelectric printheads of liquid resin and its curing with ultraviolet (UV) light	beam of UV light emitted by the generator
FDM/FFF	Fused Deposition Modeling/Fused Filament Fabrication	extrusion of molten thermoplastic material from printheads and its distribution on the working platform	heated nozzles melting the material in the form of a filament

“A pilot study to assess an in-process inspection method for small diameter holes produced by Direct Metal Laser Sintering”

Table 2

Table 2. Additive process parameters used for printing the test samples.

Machining system	EOSINT M280
Powder material	EOS MaragingSteel MS1
	EOS Aluminium AlSi10Mg
Process parameters	thickness of a single layer of a laid material: 30 µm
	type and power of a laser: a fibrous ytterbium laser of 400 W effective power
	length of a laser beam: 1060 - 1100 nm

"A pilot study to assess an in-process inspection method for small diameter holes produced by Direct Metal Laser Sintering"

Table 3

Table 3. Analysed diameters and errors for a 10 mm thick test sample made of MS1 material.

thickness of a sample G (hole length) [mm]	d_t [mm]	d_e [mm]	Δd [mm]	δ_d [%]	Feret's diameter	
					horizontal d_h [mm]	vertical d_v [mm]
10	1	0.67	0.33	33.19	0.72	0.71
	2	1.59	0.41	20.27	1.68	1.66
	3	2.53	0.47	15.64	2.60	2.63
	4	3.52	0.48	12.11	3.60	3.54
	5	4.61	0.39	7.73	4.69	4.68

"A pilot study to assess an in-process inspection method for small diameter holes produced by Direct Metal Laser Sintering"

Table 4

Table 4. Analysed diameters and errors for a 10 mm thick test sample made of EOS Aluminium AlSi10Mg material.

G sample thickness (hole length) [mm]	d_t [mm]	d_e [mm]	Δd [mm]	δ_d [%]	Feret's diameter	
					horizontal d_h [mm]	vertical d_v [mm]
10	1	0.88	0.12	12.24	0.94	0.97
	2	1.80	0.20	9.83	1.84	1.92
	3	2.58	0.42	13.84	2.65	2.70
	4	3.61	0.39	9.68	3.75	3.72
	5	4.48	0.52	10.45	4.52	4.57

"A pilot study to assess an in-process inspection method for small diameter holes produced by Direct Metal Laser Sintering"

Table 5

Table 5. Parameters of a function for determining equivalent hole diameter $d_e = a \cdot d_t$, $d_t \in [0.3, 1.5]$

thickness of a sample *G* (hole length) [mm]	directional coefficient *a*	R^2	Δy_{max} [mm]	δ_{max} [%]	RMSE [mm]
1	0.778	0.870	0.30	42.8	0.13
2	0.822	0.982	0.10	10.8	0.04
4	0.864	0.997	0.03	7.4	0.02
5	0.869	0.992	0.07	7.0	0.03

"A pilot study to assess an in-process inspection method for small diameter holes produced by Direct Metal Laser Sintering"

Table 6

Table 6. Parameters of a function for determining Feret's diameters $d_h = a \cdot d_t$ and $d_v = a \cdot d_t$, $d_t \in [0.3, 1.5]$

thickness of a sample *G* (hole length) [mm]	Feret's diameter [mm]	directional coefficient *a*	R^2	Δy_{max} [mm]	δ_{max} [%]	RMSE
1	d_h	0.892	0.911	0.14	48.8	0.09
	d_v	0.900	0.969	0.12	36.6	0.06
2	d_h	0.853	0.934	0.14	23.1	0.07
	d_v	0.904	0.956	0.11	35	0.06
4	d_h	0.879	0.993	0.05	6.2	0.03
	d_v	0.947	0.989	0.11	22.4	0.04
5	d_h	0.869	0.968	0.11	30.5	0.05
	d_v	0.969	0.988	0.07	20.4	0.04

"A pilot study to assess an in-process inspection method for small diameter holes produced by Direct Metal Laser Sintering"

Table 7

Table 7. Parameters of the linear function for calculating the equivalent hole diameter d_e for a 3 mm thick sample (d_t = 0.3 ÷ 1.5 mm) and 10 mm thick samples (d_t = 1 ÷ 5)

Thickness of a sample *G* (hole length) [mm]	**Material**	**Directional coefficient**		Δy_{max} **[mm]**	δ_{max} **[%]**	**RMSE [mm]**
3	AlSi10Mg	$\hat{a}$	0.843	0.07	14.7	0.04
		a	0.871	0.07	11.0	0.03
10	AlSi10Mg	$\hat{a}$	0.918	0.17	6.3	0.10
		a	0.892	0.10	3.6	0.05
10	MS1	$\hat{a}$	0.918	0.25	27.0	0.20
		a	0.883	0.21	24.1	0.16

"A pilot study to assess an in-process inspection method for small diameter holes produced by Direct Metal Laser Sintering"